NAVAL POSTGRADUATE SCHOOL
Monterey, California

THESIS

INVESTIGATION OF STRONG SURFACE WINDS ASSOCIATED WITH AN UPPER FRONT USING COAMPS

by

Ken Schwingshakl

September, 1997

Thesis Advisor: Patricia Pauley

Approved for public release; distribution is unlimited.

REPORT DOCUMENTATION PAGE

Form Approved OMB No. 0704-0188

1. AGENCY USE ONLY *(Leave blank)*	2. REPORT DATE	3. REPORT TYPE AND DATES COVERED
	September, 1997.	Master's Thesis

4. TITLE AND SUBTITLE	5. FUNDING NUMBERS
INVESTIGATIONOF STRONG SURFACE WINDS ASSOCIATED WITH AN UPPER FRONT USING COAMPS	
6. AUTHOR LCDR Ken Schwingshakl	
7. PERFORMING ORGANIZATION NAME(S) AND ADDRESS(ES) Naval Postgraduate School Monterey CA 93943-5000	8. PERFORMING ORGANIZATION REPORT NUMBER
9. SPONSORING/MONITORING AGENCY NAME(S) AND ADDRESS(ES)	10. SPONSORING/MONITORING AGENCY REPORT NUMBER

11. SUPPLEMENTARY NOTES The views expressed in this thesis are those of the author and do not reflect the official policy or position of the Department of Defense or the U.S. Government.

12a. DISTRIBUTION/AVAILABILITY STATEMENT	12b. DISTRIBUTION CODE
Approved for public release; distribution is unlimited.	

13. ABSTRACT *(maximum 200 words)*

On 2 April 1997, strong winds blew through the central coast of California that were accompanied by an intense jet streak and upper front. The event was analyzed with standard synoptic-scale DIFAX charts and mesoscale charts for comparison. The mesoscale model used was the Coupled Ocean/Atmosphere Mesoscale Prediction System (COAMPS) developed by Naval Research Laboratory (NRL), Monterey, California.

COAMPS captured features that were not diagnosed on the synoptic charts. Height, isotach and temperature fields showed more detail, although observations were not sufficient to completely verify the model's level of detail. COAMPS was heavily influenced by the topographic field modeling lee troughs and mountain waves along the Sierra Nevada mountains. A strong mountain wave, initiated by the upper front, ocurred in central California during this time period. The wave troughs correlated to wind maxima at the surface, including one near San Francisco Bay where winds as high as 66 mph were reported.

14. SUBJECT TERMS COAMPS, mountain waves, upper front	15. NUMBER OF PAGES 90
	16. PRICE CODE

17. SECURITY CLASSIFICATION OF REPORT	18. SECURITY CLASSIFICATION OF THIS PAGE	19. SECURITY CLASSIFICATION OF ABSTRACT	20. LIMITATION OF ABSTRACT
Unclassified	Unclassified	Unclassified	UL

NSN 7540-01-280-5500

Standard Form 298 (Rev. 2-89)
Prescribed by ANSI Std. 239-18 298-102

Approved for public release; distribution is unlimited.

INVESTIGATION OF STRONG SURFACE WINDS ASSOCIATED WITH AN UPPER FRONT USING COAMPS

Ken Schwingshakl
Lieutenant Commander, United States Navy
B.S., Marquette University, 1986

Submitted in partial fulfillment
of the requirements for the degree of

MASTER OF SCIENCE IN METEOROLOGY AND PHYSICAL OCEANOGRPHY

from the

NAVAL POSTGRADUATE SCHOOL
September 1997

ABSTRACT

On 2 April 1997, strong winds blew through the central coast of California that were accompanied by an intense jet streak and upper front. The event was analyzed with standard synoptic-scale DIFAX charts and mesoscale charts for comparison. The mesoscale model used was the Coupled Ocean/Atmosphere Mesoscale Prediction System (COAMPS) developed by Naval Research Laboratory (NRL), Monterey, California.

COAMPS captured features that were not diagnosed on the synoptic charts. Height, isotach and temperature fields showed more detail, although observations were not sufficient to completely verify the model's level of detail. COAMPS was heavily influenced by the topographic field modeling lee troughs and mountain waves along the Sierra Nevada mountains. A strong mountain wave, initiated by the upper front, ocurred in central California during this time period. The wave troughs correlated to wind maxima at the surface, including one near San Francisco Bay where winds as high as 66 mph were reported.

TABLE OF CONTENTS

I. INTRODUCTION

The headlines in three San Francisco Bay area newspapers on the morning of 3 April 1997 all pertained to strong winds that blew through the region on the 2nd. The San Francisco Examiner read "Windblown Opener", describing the San Francisco Giants opening day game on the 2nd. The Monterey Herald's "High winds blow out the lights" discussed the loss of power to more than 6000 Monterey county homes caused by the strong winds. And the San Jose Mercury News reported winds as strong as 66 mph on Mount Diablo (east of Oakland in the Diablo mountain range) under the headline "The Answer, My Friend...". These reports accompanied with the knowledge of the general synoptic situation at that time which depicted a strong jet streak in the area (see Chapter IV for details), provided the elements for follow-on work proposed by Pauley et al. (1996) regarding jet streaks, upper fronts and their influence on surface winds. This case study examines this strong low-level wind event.

The objective of the study is to compare the Coupled Ocean/Atmosphere Mesoscale Prediction System (COAMPS) analyses of the upper front/jet streak structure with available observations and with standard DIFAX charts and to diagnose the behavior of the analyzed upper front/jet streak and its effect on the low-level winds. The study will also explore mountain waves depicted by COAMPS that were generated as the upper front interacted with the Sierra Nevada range, east of the Bay area.

A. UPPER FRONTS

Upper fronts are formed by secondary circulations about jet streaks as a result of geostrophic confluence and cross-frontal geostrophic wind shear as described in Shapiro and Keyser (1990), and Keyser and Shapiro (1986). Figure 1 is a schematic depiction of these dynamic processes, which provide the framework for analyzing the secondary direct and indirect circulations responsible for jet streak propagation and upper frontogenesis. The secondary circulations caused by geostrophic confluence/diffluence without thermal considerations (Fig. 1a) are indirect in the exit region of the jet streak and direct in the entrance region. The indirect circulation forces warm air to sink acting to increase the frontal thermal gradient and vorticity while the direct circulation forces warm air to rise acting to decrease the frontal thermal gradient and vorticity. Horizontal shear modifies the location of the secondary circulations when thermal advection is present and also acts frontolytically on the cyclonic shear side of the jet streak (Fig. 1b) and frontogenetically on the anticyclonic shear side when there is an along-jet positive thermal gradient. A combination of the two is more typical with cold advection likely west of the trough axis, as shown schematically in Fig 2c. Figures 2d-f from Keyser and Shapiro (1986) also shows three other orientations and their resultant shift of the induced secondary circulations.

There have been several models of upper front structure during the past 60 years (the reader is directed to Keyser and Shapiro (1986) for a complete historical and dynamical review). Figure 3 from Keyser and Shapiro (1986) is a diagram of the

current model for analyzing upper fronts and tropopauses. The cyclonic shear zone of the upper front is on the order of 100 km, much less spread out than earlier theory suggested. This structure allows for the exchange of air parcels between the troposphere and stratosphere and also possibly the downward momentum transport of kinetic energy to low levels where boundary layer processes can mix the energy to the surface (Pauley et al. 1996). Tracers such as ozone (O_3) and potential vorticity (PV) are used to locate and identify upper fronts. Because PV is an easily derived quantity from current numerical weather prediction models, it is normally used for upper front analysis and will be used in this case study. Figure 4 from Pauley et al. (1996) is a cross-section of an upper front and jet streak with PV contours delineating the upper front.

B. MOUNTAIN WAVES

When stably stratified air is forced to rise over a topographic barrier, a disturbance is created that is carried away from the source region by gravity waves (Durran 1990). By convention, when mountains are the topographic barrier involved, the waves are referred to as mountain waves. High amplitude mountain waves can also be associated with strong surface winds that blow down along the lee slope of the mountain (Durran 1990) i.e., downslope winds. Key elements for this phenomena to occur are that the wind direction be within 30° of perpendicular to the mountain ridge line and that the upstream temperature profile exhibits a layer of strong stability near mountaintop level (Durran 1990).

A case study of a January 1972 windstorm in Boulder, Colorado was also presented by Durran (1990). Figure 5 shows the isentropic cross-sections for this event. In Fig. 5a, the atmospheric conditions are modeled using actual upstream (negative values on the x-axis) conditions that contain a strong stable layer near mountaintop level. This condition generates a strong mountain wave signature downstream from the mountain. In Fig. 5b, the stable layer is removed from the model run with all other parameters the same. Notice the absence of the wave signature downstream from the mountain indicating that the stable layer interaction with the mountain initiated the wave. In the case presented in this thesis, the upper front provided the stable layer for this interaction.

The thesis is organized as follows. The COAMPS data assimilation system used in this research is briefly described in Chapter II, to the extent necessary for basic understanding. The methodology presented in Chapter III identifies the FORTRAN program used to run and plot the data fields from the model, followed by a synoptic overview in Chapter IV using standard charts to describe the broad scale atmospheric conditions during the case study. A comparison of COAMPS model data to the standard chart data is then conducted in Chapter V followed by a discussion in Chapter VI on the gravity/mountain waves depicted by COAMPS in this case. Finally results of the study and recommendations for follow-on work are presented in Chapter VII.

II. COAMPS OVERVIEW

COAMPS, the Coupled Ocean/Atmosphere Mesoscale Prediction System, consists of an atmospheric nonhydrostatic model and a hydrostatic ocean model. This section will provide a brief description of the atmospheric model, the only component of COAMPS used in this study. The COAMPS atmospheric model is designed for either idealized or real-data simulations. This case study uses real-data assimilation which consists of data quality control, analysis, initialization and forecast components which are briefly described below. For a detailed account of the model, the reader is directed to Hodur (1997), the source for this overview.

A. GRID CONFIGURATION

Polar stereographic, Mercator, spherical grid or Lambert conformal projections are available with the model. An Arakawa C grid on a Lambert conformal projection is used for this case study. The model utilizes nested grids, with up to nine meshes allowed provided there is a 3:1 reduction in grid spacing between grids. For this case study a two-mesh nested grid was used, 81 km for the coarse grid and 27 km for the fine grid. Detailed analysis was conducted on the 27 km inner grid. The model uses the sigma-z vertical coordinate scheme consisting of 30 levels with approximately 9-10 levels in the planetary boundary layer.

B. INITIAL CONDITIONS

Several surface fields must be initialized before running COAMPS. Terrain height is obtained from the U.S. Navy 20′ resolution terrain field (approx. 20 km) or

the Defense Mapping Agency (DMA) Digital Terrain Elevation Data (DTED) level 1 data (100 m resolution). The U.S. Navy 20′ terrain field was used for this case study as seen in Fig. 6. Surface albedo, roughness and ground wetness are also specified primarily by using monthly climatological global fields bilinearly interpolated to the COAMPS grids. Ground temperature is obtained from a surface energy budget over land and NOGAPS analyzed surface temperature (held constant for model integration cycle) over water.

Extensive quality control (QC) programs (Baker 1992) are used to check observational data for errors. The data that pass the QC checks are then mapped to the model grids using a multivariate optimum interpolation (MVOI) analysis technique (Lorenc 1986 and Barker 1992). While processing data for this case study, it was discovered that there was a problem with the COAMPS implementation of the MVOI scheme for the inner mesh. Briefly, the MVOI scheme was performed using four volumes for the inner mesh that did not overlap. First-order discontinuities at the edge of the analysis volumes were seen in this case, because the western two volumes used the data-sparse algorithm, while the northeastern volume used the data-rich algorithm. When the volumes were assembled, derivative quantities such as divergence had large values at the interface between analysis volumes, bisecting the domain shown in Fig. 6 in both x and y directions. To solve this problem, the volumes were made to overlap so that each region sampled had a similar data distribution resulting in a more continuous analysis increment field (Holt, personal communication). Observations used in this study were obtained from radiosondes,

pibals, AIREPS, ACARS, SSM/I, surface obs, cloud track winds, DMSP and NOAA satellites.

An incremental or full update cycle can be used for the analysis. In the incremental update cycle, which was used for this study, the analyzed increment fields are interpolated from the 16 mandatory pressure levels from 1000 to 10 mb to the model's sigma-z vertical levels and added to the model's sigma-z level first guess, preserving the model's vertical structure. Once the initial fields are obtained, they must be initialized using a variational method to reduce the generation of spurious high-frequency oscillations and to assure that vertical propagating sound waves are not generated.

C. FORECAST MODEL

Lateral boundary conditions for the COAMPS coarse grid are obtained from the most recent Navy Operational Global Atmospheric Prediction System (NOGAPS) forecast. The NOGAPS fields are horizontally interpolated using a bicubic spline to the COAMPS coarse grid, then interpolated in the vertical to the model vertical coordinate. The grids utilize one-way interaction, i.e., outer to inner for interior boundary conditions. Second-order numerical differencing is used throughout the model except for diffusion which is fourth-order. The time differencing scheme used is split explicit.

Clouds and precipitation are treated differently depending on the grid spacing. Below 10 km resolution, COAMPS has explicit moist physics (Rutledge and Hobbs 1983) and performs as a cloud model. Above 10 km, as in this case, COAMPS uses

explicit treatment of the moist physics for nonconvective clouds and precipitation and the Kain - Fritsch (Kain 1990, Kain-Fritsch 1993) cumulus parameterization for convective clouds and precipitation. The Louis et al. (1982) scheme is used to model surface fluxes, the Harshvardan et al. (1987) method is used for atmospheric radiation and, the Deardorff (1980) parameterizations for subgrid-scale mixing is used.

D. COAMPS SPECIFICS FOR APRIL 1997 CASE

For the case presented in this thesis, COAMPS was run in data assimilation mode using a 6-h incremental update cycle, beginning 0000 UTC 1 April 1997. A NOGAPS analysis was used for the background at the initial time, after which a 6-h COAMPS forecast was used as background. A two-nest version was used with 61 x 61 grid points on the outer 81 km resolution grid and 73 x 73 grid points on the inner 27 km resolution grid, both centered at 35°N 120°W on a lambert conformal projection. Thirty vertical levels were used.

III. METHODOLOGY

The sigma-level COAMPS analyses were post-processed to pressure levels at a 50 mb interval from 1050 mb to 100 mb and displayed using FORTRAN code that was developed by Prof. P. M. Pauley (Naval Postgraduate School) and Dr. E. H. Barker (Naval Research Laboratory, Monterey) for previous case studies including the 1991 dust storm. The code was revised to accept COAMPS data rather than NORAPS (Navy Operational Regional Atmospheric Prediction System) data. Namely the vertical coordinate definition, the grid dimensions, and the input routines needed to be revised to use the COAMPS fields. The plotting portion of the program is based on National Center for Atmospheric Research (NCAR) graphics.

This diagnostics package can compute sea level pressure using several different algorithms. The Mesinger (1990) technique was chosen as being less noisy than the other possibilities. In this technique, temperatures are interpolated horizontally in below-ground regions by setting the Laplacian of the temperature field to zero at below-ground points and using the neighboring above-ground points on a given pressure level as boundary conditions. The solution was obtained by sequential overrelaxation. The resulting temperatures were used to compute heights or pressure surfaces at below ground points. The sea-level pressure values were then obtained by extrapolating downward from the nearest pressure surface that is above sea-level.

The data for each date-time-group were transferred using ftp from Naval Research Laboratory (NRL) in Monterey, California and then unpacked. The diagnostics code was run separately for each date-time-group with several choices available for output. Plan-view charts with conventional fields such as heights, winds, vertical motions, and temperatures were primarily used. Vertical cross-sections were also plotted and used for diagnosing theta surfaces, potential vorticity, mountain waves, and the interaction of the upper front with topography.

IV. SYNOPTIC OVERVIEW

This chapter describes the synoptic situation that encompasses the high wind event in central California on 2 April 1997. National Center for Environmental Prediction (NCEP) ETA DIFAX charts at standard levels will be used to describe the synoptic-scale features' initial state and evolution during the period.

A. 0000 UTC 1 APRIL

A high amplitude longwave pattern exists from 850-300 mb over the eastern North Pacific through the Northern Plains of the United States at this time (Figs. 7-10). The ridge axis of interest to this case study is centered at approximately 140 W extending well into the Gulf of Alaska. The trough axis of interest lies along 120 W over eastern Washington and Oregon with the base of the trough over central California and southern Nevada. A second ridge is centered at 95 W along the western Minnesota border.

At 300 mb (Fig. 7), observations indicate a 65 m/s jet streak is slightly downstream of the ridge axis while 45 m/s winds extend southward to the northern California border. Note that the eta analysis is too weak, with a jet streak maxima of only 110 kt, approximately 55 m/s. Although a closed low has not yet formed in the base of the trough, a -35° C cold pocket is located over central and eastern Oregon at 500 mb (Fig. 8) with weak cold air advection into the trough base. Moderate warm air advection is occurring at the ridge axis.

At the surface (Fig. 11), a 1035 mb high over the eastern north Pacific and a 1004 mb low located in southern Nevada is causing a moderate pressure gradient over California with the strongest gradient in the southwestern part of the state. A wavy cold front, supported by the shortwave at 850-700 mb (Figs. 9 and 10), extends southwest from northeastern Montana through southern California.

B. 1200 UTC 1 APRIL

During the following 12 h, the ridge builds and moves east about 5° developing a slight tilt to the northeast. The trough, however, is quasi-stationary and does not deepen. The 65 m/s jet streak at 300 mb (Fig. 12), verified by the Salem, Oregon rawinsonde observation, has propagated down the coast to a location over western Washington and British Columbia aligned north to south. The -35° C cold pocket at 500 mb (Fig. 13) has also moved slightly to the east over western Idaho. 700 mb shows no significant features at this time or for the remaining valid times and is therefore omitted for the rest of the overview.

At 850 mb (Fig. 14) a lobe of the ridge, oriented west to east, has built eastward through the central Rocky Mountain region causing the height contours to lie west to east and generating flow normal to the Sierra Nevada range. The trough associated with the embedded shortwave remains through the southwest along with a quasi-stationary isotherm pattern, signaling a stalled front in the region. Height falls at San Diego are 20 m at this level but only 10 m at 500 mb (Fig. 13), reflecting the low-level frontal feature.

The surface high is quasi-stationary building to 1038 mb while the low filled to 1008 mb and moved into northwestern Arizona (Fig. 15). The isobars become oriented northeast to southwest over California with an inverted trough analyzed by NCEP over eastern California and are more evenly spaced than 12 h earlier. The wavy front is quasi-stationary in the southwest but pushed farther east in the central U.S. by the west to east ridge lobe described at 850 mb.

C. 0000 UTC 2 APRIL

The ridge continues to build to the northeast and the trough deepens slightly, gaining a much more prominent northeast to southwest tilt during this 12 h period. The second ridge builds sharply back to the northwest, enhancing the blocking pattern. The 65 m/s jet streak at 300 mb (Fig. 16) centered over central Oregon also becomes oriented northeast to southwest with 50 m/s winds extending to Oakland. Observations to confirm the strength of the jet streak were not available.

At 500 mb (Fig. 17) a 5440 m closed low is analyzed over southern Nevada, coincident with the -35° C cold pocket. The temperature gradient becomes stronger over central California while heights begin to fall significantly in southern California with San Diego reporting a 70 m fall during the past 12 h.

The shortwave trough through the southwest at 850 mb (Fig. 18) deepens slightly but remains quasi-stationary along with the isotherm pattern. Enhanced lee troughing is evident through central California. Height falls range from 19 m at San Diego to 44 m at Flagstaff.

The 1038 mb high at the surface (Fig. 19) moves northeast and the low over northern Arizona along the quasi-stationary wavy front deepens to 1003 mb, producing a somewhat tighter pressure gradient. Some troughing is evident along the San Joaquin Valley, a reflection of the lee side trough at 850 mb (Fig. 18).

D. 1200 UTC 2 APRIL

The longwave pattern has changed little in the previous 12 h. The trough moves slightly to the southwest and is now anchored by the newly formed 8920 m closed low at 300 mb (Fig. 20) over extreme southwestern Nevada. The strongest reported wind at 300 mb is 57 m/s out of the north-northeast at Oakland. The jet streak is analyzed accordingly for speed and is depicted as having elongated and begins to wrap around the closed low.

At 500 mb (Fig. 21), 180 m height falls occur at San Diego as the closed low moves southwestward, becoming nearly vertically stacked with the closed low at 300 mb and lower levels.

Deep height falls are also taking place at 850 mb (Fig. 22) over the southwest. San Diego shows a 41 m height fall for the past 12 h as the closed low becomes entrenched in the region and is coincident with the upper levels. The lee side trough through central California is enhanced as the gradient tightens from north to south.

The quasi-stationary surface high has weakened to 1037 mb but the quasi-stationary low along the wavy front has deepened to 1000 mb, thus maintaining the relative isobaric packing (Fig. 23). The inverted trough appears to be closer to the coast, rather than over the Central Valley area.

E. 0000 UTC 3 APRIL

A significant change in the longwave pattern can be detected at this time. The second ridge to the east begins to break down as the previously quasi-stationary shortwave gains energy, moves to the northeast and suppresses the second ridge. The 300 mb pattern around the closed low remains virtually unchanged as the low slowly drifts to the southwest (Fig. 24). A 55 m/s jet streak, aligned as before, is analyzed by NCEP, supported by a 52 m/s report from Oakland. A weaker 45 m/s jet streak is depicted southeast of the closed low, possibly related to the jet streak propagating around the low.

The closed low at 500 mb (Fig. 25) also drifts to the southwest and fills by 20 m. Height rises are found throughout the entire region. Although Oakland is still reporting strong 45 m/s northeasterly winds, the tightest temperature and height gradient is located well off the southern California coast, in an area of no upper air observations.

The isotherms associated with the quasi-stationary shortwave at 850 mb have moved through the area to the southeast (Fig. 26). They have been isolated from the shortwave by a bubble high that has split away from the eastward protruding lobe of the offshore ridge that was discussed earlier. The height contours have realigned slightly to the northeast, weakening the lee side trough.

The surface pressure gradient has eased in southern California as the low along the wavy front has moved to the northeast over northwest New Mexico and filled to 1004 mb (Fig. 27). A weak inverted trough is analyzed from southern to

central California along the valley region. The 1037 mb high remains in place and is keeping the gradient tight in northern California.

V. COAMPS COMPARISON

Although the operational NCEP charts such as shown in the previous chapter are produced from 48 km eta model, the fields are highly smoothed before producing the DIFAX graphics. Consequently, the 27 km mesh of the COAMPS model has more detail than the standard NCEP charts. Height fields and isobars show more small amplitude features but were in general agreement as to location of the contours. Wind fields show more mesoscale structure than are typically analyzed at synoptic scales, and other parameters such as temperature also show similar levels of detail (not shown). Higher resolution observations were normally not sufficiently available to verify this level of mesoscale detail, leaving questions as to what was real and what features were model artifacts. The biggest difference between the synoptic and mesoscale analyses was the topographic influence for COAMPS, namely, COAMPS depicted mountain waves and small-scale lee troughs that were not apparent on the NCEP charts.

A. TIME SERIES COMPARISON

The 300 mb and surface charts were chosen for this comparison because they are the essence of this study. 300 mb provides the best level to examine the jet streak and the surface represents the meteorological effects that are best recognized.

1. 0000 UTC 1 April

Figure 28 shows the 300 mb COAMPS analysis chart with heights as solid lines, isotachs are shaded in increments of 5 m/s starting at 30 m/s, and observations

are also in m/s with flags equal to 25 m/s, a full barb equal to 5 m/s, and a half barb equal to 2.5 m/s (Note: this convention is maintained throughout the paper.). Comparing this chart to the NCEP chart (Fig. 7), one can see the obvious differences in the representation of the isotachs. NCEP shows a smooth, elongated 90 kt (approximately 45 m/s) jet streak extending well into central California whereas COAMPS depicts a more detailed pattern with the 45 m/s isotach barely reaching the northern California coast. Rawinsonde observations from Oakland (37.5 m/s) and Salem (37.5 m/s) seem to verify COAMPS depiction.

The COAMPS surface chart (Fig. 29) shows good agreement with NCEP (Fig. 11) regarding isobar location and general surface pressure pattern. Isobars are solid lines, isotachs are shaded as before but begin at 15 m/s vice 30 m/s, and observations are in m/s as before. There is one noteworthy difference however. COAMPS shows a small-scale trough forming in the lee of the Sierra Nevada range in north-central California, while NCEP shows straight isobars with no troughing evident.

2. 1200 UTC 1 April

The irregular isotach pattern is again evident on the COAMPS 300 mb chart (Fig. 30). The maximum isotach of 55 m/s (approximately 110 kt) is just touching the northern California border whereas the NCEP 110 kt isotach extends almost as far south as San Francisco (Fig. 12). Because the Salem rawinsonde is missing wind direction and speed, verification of the COAMPS maximum isotach is not possible. It also appears that the 30 m/s isotach extending south into the Bay area on the

COAMPS chart forced the 110 kt isotach farther south than it should have on the NCEP chart due to smoothing.

The surface charts are beginning to show disagreement in the isobar pattern over land. Note the small-scale troughs that COAMPS is depicting in the lee of the Sierra Nevada range and along the coast (Fig. 31). NCEP shows broad inverted troughing extending along the coast with a manually analyzed "trof" (Fig. 15) in the approximate location of the COAMPS lee trough. This suggests that COAMPS is successfully analyzing a feature that is known to be present but not properly represented by the synoptic-scale DIFAX chart.

3. 0000 UTC 2 April

The models are generally in agreement as to the location and intensity of the jet streak at this time. Both COAMPS (Fig. 32) and NCEP (Fig. 16) show the 55 m/s (approximately 110 kt) isotach over north-central California with stronger winds embedded upstream. Although NCEP depicts a slightly stronger jet maximum (130 kt) than COAMPS (60 m/s) , observations are not sufficient or available to verify either. Of particular interest however, is the onset of a small-scale trough that is analyzed by COAMPS in the lee of the Sierra Nevada range. The trough is accompanied by a distinct wavy pattern of the isotach field in the same region suggesting possible correlation of these two features.

The surface differences are the same as 1200 UTC 1 April except that NCEP (Fig. 19) is no longer indicating a "trof" in the lee of the Sierra Nevada range. On the COAMPS chart (Fig. 33), three separate wind maxima are being depicted in

northern California with two over the land and one broad maximum off-shore. The two maxima over land seem to be located in conjunction with the two small-scale troughs that were identified earlier. The next valid time, 1200 UTC 2 April, proves to be the most interesting and dynamic in the sequence and will be the primary focus for the remainder of this paper.

B. UPPER-LEVELS AT 1200 UTC 2 APRIL

Starting at 300 mb, compare Fig. 20 the NCEP chart with Fig. 34, the COAMPS chart for the same valid time, 1200 UTC 2 April. The NCEP chart shows a smooth, elongated 110 kt jet streak extending through central California. On the COAMPS chart, note again the more detailed pattern in the isotach field and the two distinct jet maxima of 65 m/s, approximately 10 m/s stronger than NCEP has analyzed.

However, the observational network is not dense enough to verify the strength or the location of these jet maxima. Mesoscale details such as these come from the six-hour COAMPS forecast that was used as background for the analysis. The Reno rawinsonde observation is within the isotach maximum at the California/Nevada border, but has no wind observation. The assumption is that the windspeed is strong and the balloon was blown away. Also note that sometimes even where there are observations, significant differences between the analysis and the observations exist. The Oakland rawinsonde observation has a windspeed of 57.5 m/s but is inside the 60 m/s isotach. The opposite situation occurs at Vandenburg which has an observation of 60 m/s but is just inside the 50 m/s isotach. However, the latter

observation is approximately 100 km west of aircraft observations of 27.5 and 17.5 m/s in a location where the analysis is between 30 and 35 m/s. Unable to determine if these observations are used in the analysis, one can only conclude that the analysis possibly has problems depicting this large horizontal shear. The NCEP analysis portrays values of approximately 53 m/s and 38 m/s, respectively, at these two locations which yields an even weaker horizontal shear than COAMPS. In regions with weaker wind shear, the COAMPS analysis draws more closely to the observations, e.g., Medford, Oregon.

At 500 mb, for the same valid time, NCEP has analyzed straight contours through north-central California and Baja, California (Fig. 21). Compare this with the COAMPS chart (Fig. 35), which shows small-scale troughing of the height contours in both north-central and Baja, California, regions of considerable topographic variability (Fig. 6). At this level, the rawinsonde observations at Oakland, Vandenburg, and Reno are in good agreement with the isotachs. The two charts are in very good agreement as to the general location of the height contours and the closed low over southern California. This type of agreement was prevalent throughout the case at upper levels.

C. LOWER LEVELS AT 1200 UTC 2 APRIL

Examination of the surface charts for 1200 UTC 2 April yields a dramatic difference compared to the NCEP chart. Figure 23, the NCEP chart, has a broad inverted trough analyzed that extends over the adjacent offshore region. The COAMPS surface chart (Fig. 36) has two distinct small-scale troughs analyzed, one

in the lee of the Sierras and one over the coast in northern California. The automated analysis system used to generate NCEP's surface chart does smooth through small-scale features, accounting for some of the difference. But even so, the observations are not dense enough to confirm the small-scale troughs. Since the troughs are associated with terrain features, reduction error might be playing a role. However, this SLP analysis utilizes the horizontal reduction techniques proposed by Mesinger (1990) which tends to yield less reduction error than conventional vertical extrapolation techniques (Mesinger and Treadon 1995, Pauley 1997). It is noteworthy that the western of these two small-scale troughs is roughly below the small-scale 500 mb trough, suggesting that this feature has vertical continuity.

Further analysis of the COAMPS surface chart reveals the interesting features in the surface isotachs in northern California. The broad windspeed maximum is located off shore, similar to that seen in Pauley et. al. (1996). Notice again the distinct wind maxima that occur over the land in conjunction with the small-scale troughs. The observational network is not sufficient to explicitly verify these features, but there is a 15 m/s observation in north-central California in proximity to the wind maxima. The 700 mb COAMPS chart (Fig. 37) shows the same pattern of small-scale troughs and wind maxima as the surface chart. The correlation of the maxima at these two levels suggested the existence of some type of disturbance; the location of the disturbance in the lee of the Sierra suggests a mountain wave.

VI. GRAVITY/MOUNTAIN WAVES

A. UPPER FRONT INTERACTION

Figure 38 shows the 500 mb vertical velocity (w) field (shaded at 5 cm/s increments) and the height contours at 1200 UTC 2 April, the same time that the three separate low-level wind maxima are the most dominant. A negative value implies downward vertical motion, positive upward. There is clearly strong downward and upward motions in the northern California region downstream of the Sierras. Upon further examination, the downward vertical motion maxima are in approximately the same location as the lower level wind maxima that were discussed earlier. Also notice the vertical motion maxima in Baja, California, another region that has a complex terrain (Fig. 6). This vertical motion pattern suggests the presence of a mountain wave as it would be depicted in plan view. Furthermore the correlation between the intense westernmost downward motion maximum and the small-scale 500 mb trough, suggests that the troughing is a hydrostatic response to adiabatic warming associated with the mountain wave. The 500 mb temperature gradient (Fig. 39) agrees with this premise. Notice the strong gradient (shaded at increments of 3 K/100 km starting at 3 K/100 km) associated with the western most downward maximum. The isotherms, represented by thin solid lines at 2°C, also show tighter packing in the same area. This in turn would strengthen the jet streak due to thermal wind considerations thereby enhancing the upper front as well, representing positive feedback. The jet streak at 300 mb does in fact strengthen from

0000 UTC (Fig. 32) to 1200 UTC (Fig. 34) 2 April as can be seen by comparing the two charts. The increase in speed would also tend to strengthen the secondary circulations associated with the jet making for a stronger upper front. The stronger the upper front, the stronger the stable layer which implies an enhanced mountain wave completing the cycle.

Figures 40 and 41 depict a cross-section through north-central California at 1200 UTC 2 April in plan view and the vertical view. The shaded areas are the isotachs at 5 m/s increments, the dashed lines are isentropes and the dark solid lines represent PV Units (PVU) of 1.6 for the lower and 3.0 for the upper line. The 1.6 PVU line is representative of the tropopause and upper front signature. Comparison of this cross-section and that of the Boulder windstorm examined by Durran (1990)(Fig. 5) show remarkable similarity. Both show the tight packing of the isentropes in the stable layer upstream of the mountaintop and the strong wave pattern in the isentropes downstream. The tight packing of the isentropes at tropopause level over the first crest of the mountain wave downstream of the mountain peak is also present in both figures. The isotachs in Fig. 41 also show the wave pattern. This field is not depicted in the Boulder case so direct comparison is not possible. Oakland and Reno rawinsonde data support the isotachs but cannot resolve the wavy structure. Notice that a strong upper front is not indicated by the PVU contours at this time even though the stable layer is present upstream of the mountain. Additional cross-section analysis is necessary to resolve the influence of the upper front in this case.

A cross-section through the same plane but at 0000 UTC 2 April is shown in Fig. 42. There is a strong upper front signature defined by the 1.6 PVU contour that intersects the mountain topography. Notice however that the wave pattern is not as dominant as it is at 1200 UTC 2 April (Fig. 41). So, at this time, 0000 UTC 2 April, the upper front, a stable layer by definition, interacts with the Sierra Nevada range and excites a mountain wave as defined by Durran (1990). As the upper front continues to propagate with the jet streak from 0000 UTC to 1200 UTC 2 April (see synoptic overview), the strong frontal signature is no longer present in this cross-section plane, but the resultant wave remains and is supported by a stable layer upstream that is not connected to the dominant upper front.

VII. CONCLUSIONS

This thesis presented a case study of an upper front and mountain wave event that contributed to high winds in central California on 2 April 1997. This chapter identifies the primary results of the study derived from the COAMPS analyses.

A. UPPER FRONT

The upper front associated with the jet streak that moved through northern and central California on 2-3 April, 1997 excited a mountain wave just north of Lake Tahoe, as the front interacted with the Sierra Nevada range in that area. The stable layer, a signature of an upper front, was near mountain-top level and on the upwind side, a necessary situation to generate mountain waves. The wave initiated in this region extended to offshore regions west of San Francisco. The wave interacted with the surface in two places as evidenced by the two distinct wind maxima at the surface that were coincident with the wave pattern. Thus the high surface winds generated in those areas were at least in part due to higher velocity winds aloft being brought to the surface by the wave.

Although not directly associated with the upper front, downslope winds were also modeled along the lee of the Sierras far to the south. The impact of the downslope winds on the total surface wind field is not exactly known. Adiabatic warming of the descending air would reduce the surface pressures on the lee side and would result in stronger winds due to the tightening of the pressure gradient.

B. DIFFERENCES FROM 1991 "I 5" DUST STORM

The biggest difference between this case and the 1991 case was the direction of the upper level winds and accompanying jet streak. In the 1991 case, the upper-level winds were from the north-northwest whereas in this case the winds and jet streak are from the northeast. The northeasterly flow caused the jet streak and upper winds to interact with the Sierra Nevada range producing mountain waves and disrupting the flow. The 1991 winds were nearly parallel to this mountain range and had no obvious interaction with the topography.

A second difference that may also account for the absence of mixing upper-level winds to the surface was the stability of the lower levels. This case had a more stable lower layer than the 1991 case which may have inhibited mixing.

The time of year and climatological conditions are different as well. The 1991 dust storm occurred in early November after a period of unprecedented drought in California. This case occurred in early April following an abnormally wet winter. The degree of soil heating based on moisture and vegetation would be less for this case resulting in less heating of the boundary, also thereby increasing the stability of the lower levels as observed.

C. COAMPS AND MOUNTAIN WAVES

Because COAMPS has only been in use for a short time and is not yet operational, there is not a lot of information as to how accurately the model depicts meteorological phenomena. However, one case study was done that analyzed the ability of COAMPS to model mountain waves. The case study by Doyle et al. (1995)

describes how COAMPS successfully modeled a downslope wind and mountain wave event that occurred in Oppdal, Norway in January 1995. Although in this case the stable layer was a surface warm front, cross-section comparison between that event and the April 1997 event are very similar. Figure 43 shows four panels depicting the Oppdal wind storm. In Fig. 43a, isentropes are presented with the underlying topography. Compare this to the isentropic pattern for the April 1997 case (Fig. 41) and notice the obvious similarity in the theta surface pattern. The Oppdal cross section was run at 3 km resolution vice 27 km which accounts for the smaller amplitude waves shown. The other three panels of Fig. 43 show the geographic, topographic and mesh boxes (Fig. 43b) used for Oppdal, the cross section of horizontal wind speed (Fig. 43c), and the cross section plane in the plan view (Fig. 43d).

There are differences between the two cases, namely the vertical position of the stable layer and the finer mesh used in the Oppdal case. However, the underlying premise that COAMPS has been known to successfully model mountain wave events cannot be refuted. This gives one greater confidence in the model output for the April 1997 case, even though observations remain insufficient to verify the event.

VIII. RECOMMENDATIONS

The following recommendations are provided for possible follow-on work to this case or similar ones. First, seek additional non-conventional observations that may be available for the area of concern to verify the model output for this case, especially the high surface winds. Although several of these sources were examined, more may be available through other networks or organizations.

Second, run this case with a higher resolution for COAMPS. At a 9 km mesh for instance, smaller amplitude features may be analyzed. In addition, a 100 m terrain field could be used instead of the 20 km used in this study due to the finer resolution of the inner most grid.

Third, compare the COAMPS output with those of other mesoscale models such as the 10 km eta model from NCEP or the MM-5, run locally at the Naval Postgraduate School. Not only could this help to verify the COAMPS output, but it would also provide direct comparison of a non-hydrostatic model (COAMPS or MM-5) to a hydrostatic model (10 km eta) and their ability to model mountain waves and downslope winds.

Fourth, run COAMPS forecast fields out through tau-24 or tau-36 to determine how well the model can forecast this case and also see how far in advance the model can successfully predict this event.

Finally, use the COAMPS or other mesoscale models to examine other northeasterly wind events over the Sierra Nevada range and see if they also yield

similar patterns to what occurred in this case. Differences, if there are any, would be useful to forecasters to better their prediction knowledge and skills for mountain wave and downslope wind events.

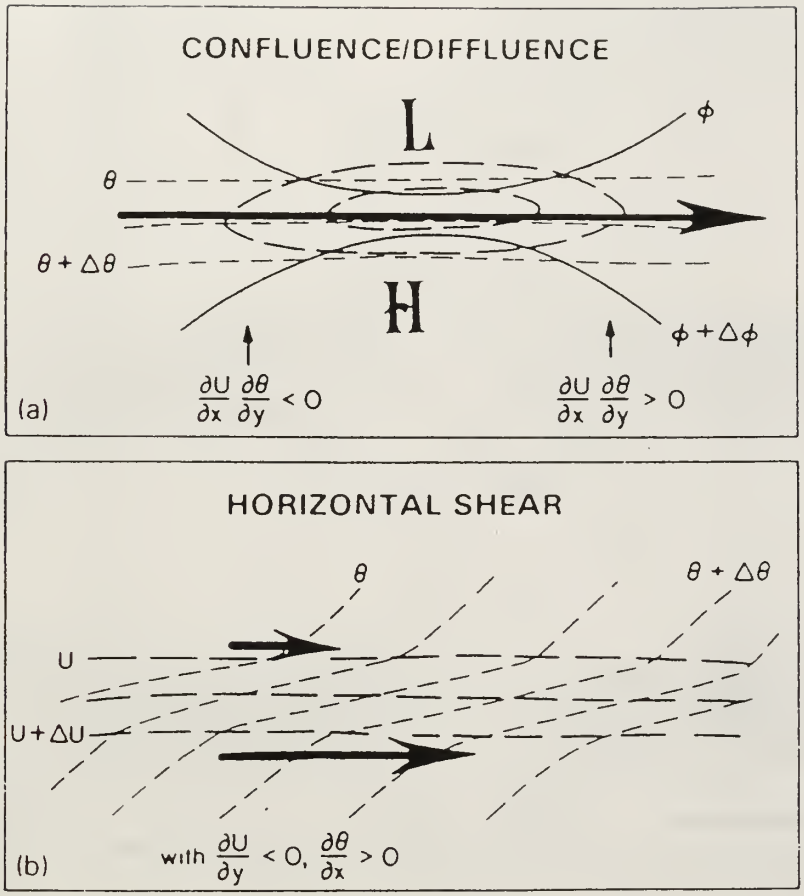

Fig. 1. Schematic depictions on a constant pressure surface, of straight frontal zones characterized by (a) confluence and diffluence associated with a jet maximum, and (b) horizontal shear in the presence of a positive along-front thermal gradient. Geopotential height contours, thick solid lines; isotachs of the along-front geostrophic wind component U, thick dashed lines; isentropes, thin dashed lines. Heavy arrows indicate the jet axis in (a) and the sense of cross-front shear of the along-front wind component in (b). (from Shapiro and Keyser 1990, Fig. 10.6)

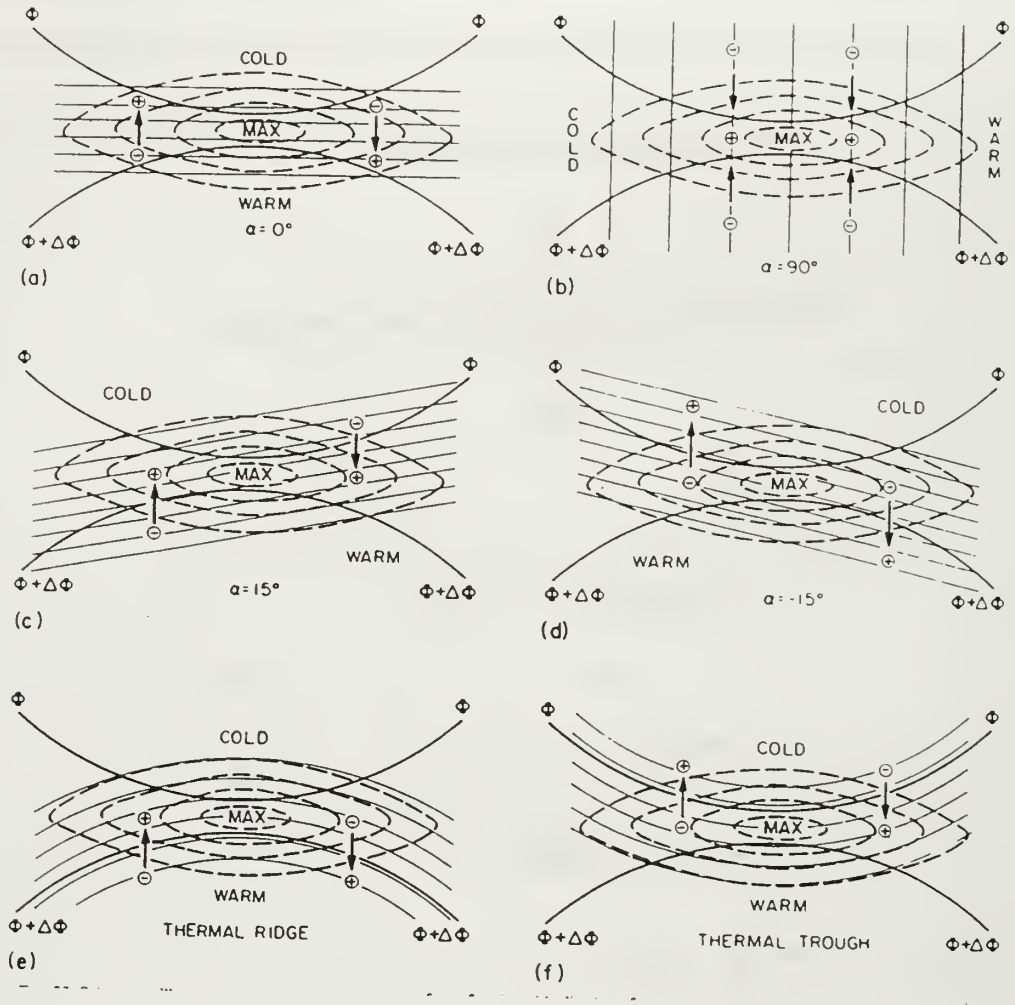

Fig. 2. Schematic illustration on a constant pressure surface of various idealized configurations of potential temperature and along-front geostrophic wind for straight upper-tropospheric jet maximum. Thick solid lines, geopotential height contours; thick dashed lines, isotachs of the along front wind component; thin solid lines, isentropes or isotherms; thick solid arrows, sense of cross-front ageostrophic wind component at level of maximum wind; plus and minus signs, sense of mid-tropospheric pressure-coordinate vertical velocity. (a) Pure confluence and diffluence in the absence of along-jet thermal advection; (b) pure horizontal shear with $\partial\theta/\partial x > 0$ in the absence of the effect of confluence and diffluence. (c)-(f) Mixed cases of confluence/diffluence and horizontal shear: (c) along-jet cold advection, (d) along-jet warm advection, (e) jet in thermal ridge, (f) jet in a thermal trough. (from Keyser and Shapiro 1986, Fig. 23)

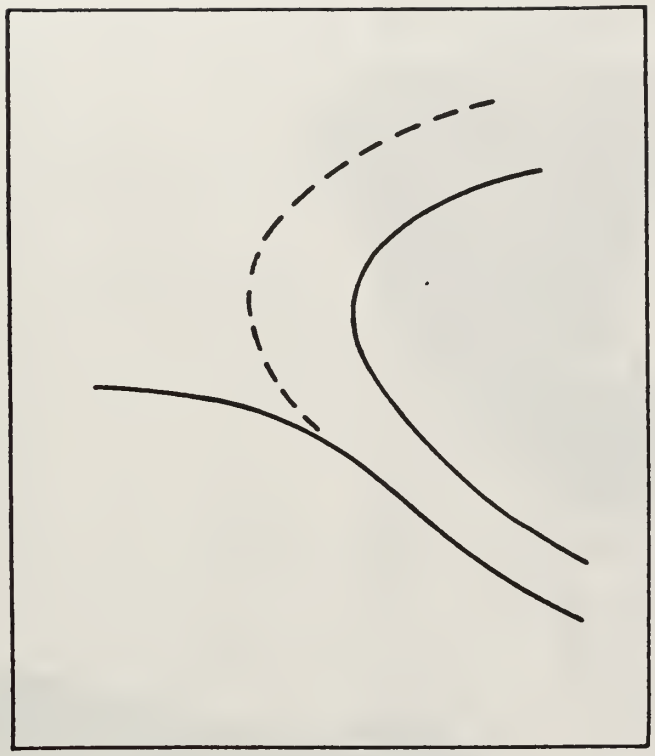

Fig. 3. Schematic diagram of the present-day model for analyzing upper-level fronts and tropopauses. Solid lines denote frontal and tropopause boundaries; dashed line depicts the boundary of cyclonic shear zone in the lower stratosphere. (from Keyser and Shapiro 1986, Fig. 6)

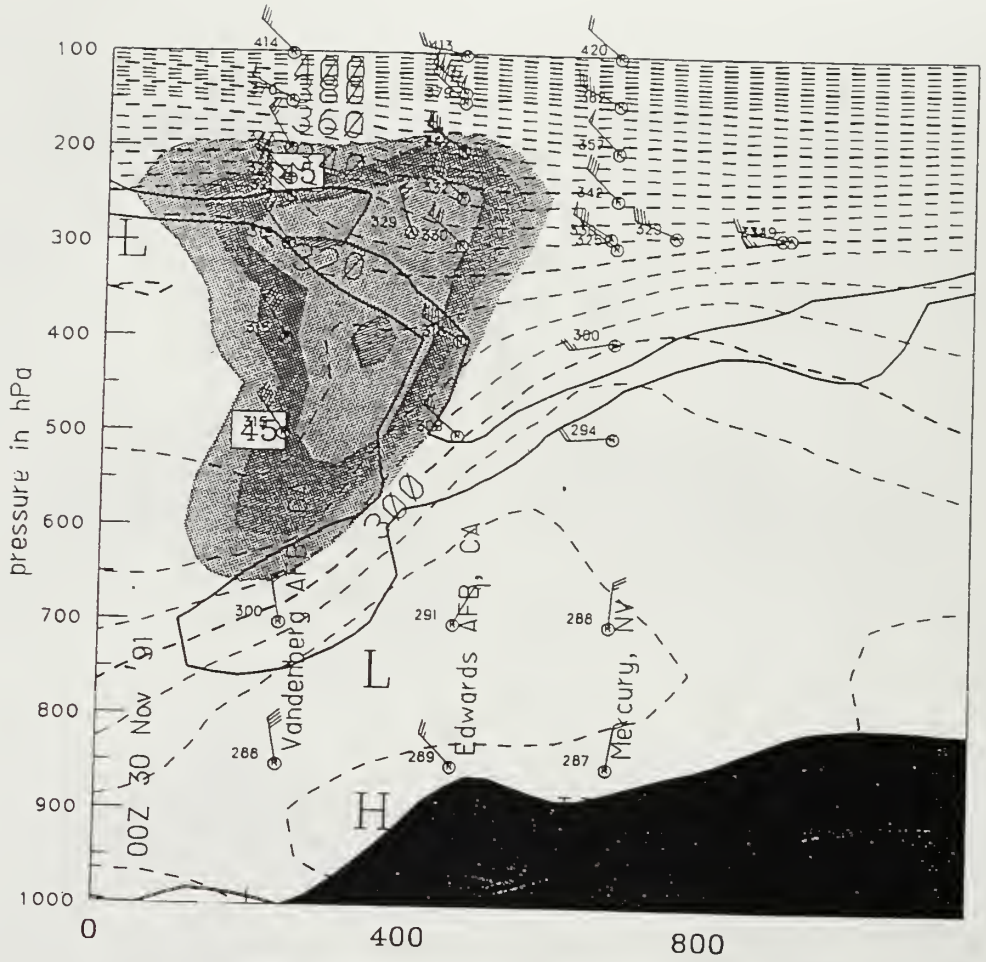

Fig. 4. Cross section from the 1991 dust storm case (Pauley et al. 1996). Pressure is the y-axis and distance along the cross section is on the x-axis. Isentropes are dashed lines, isotachs are shaded at 5 m/s increments, and the bold solid lines are 1.6 (lower) and 3.0 (upper) PVU.

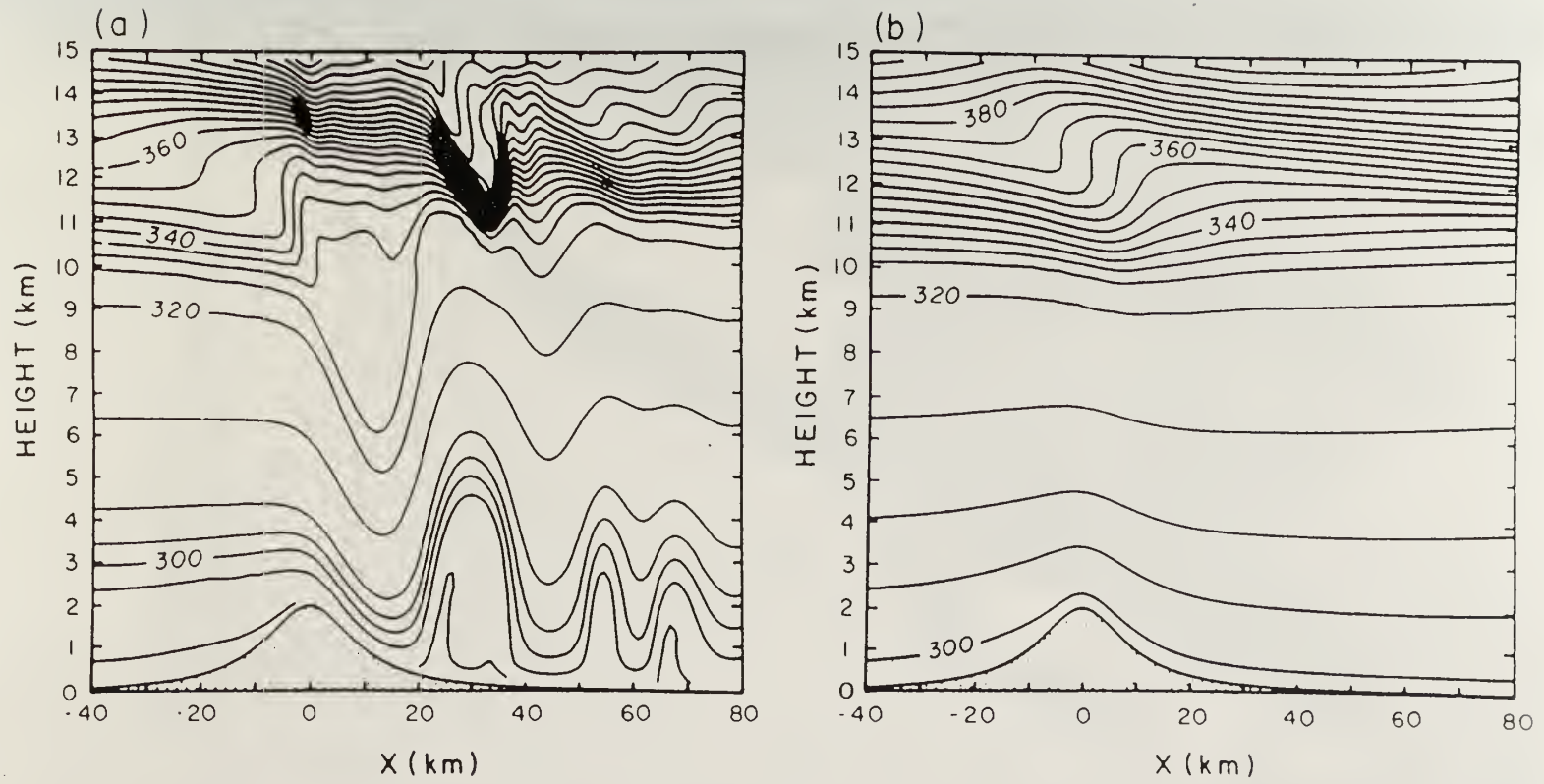

Fig. 5. (a) Isentropes form a simulation of the 11 January 1972 Boulder windstorm using the upstream conditions observed at Grand Junction at a model time of 12,000 s. (b) As in (a), except that the upstream sounding has been modified to remove the elevated inversion. (from Durran 1990, Fig. 4.10)

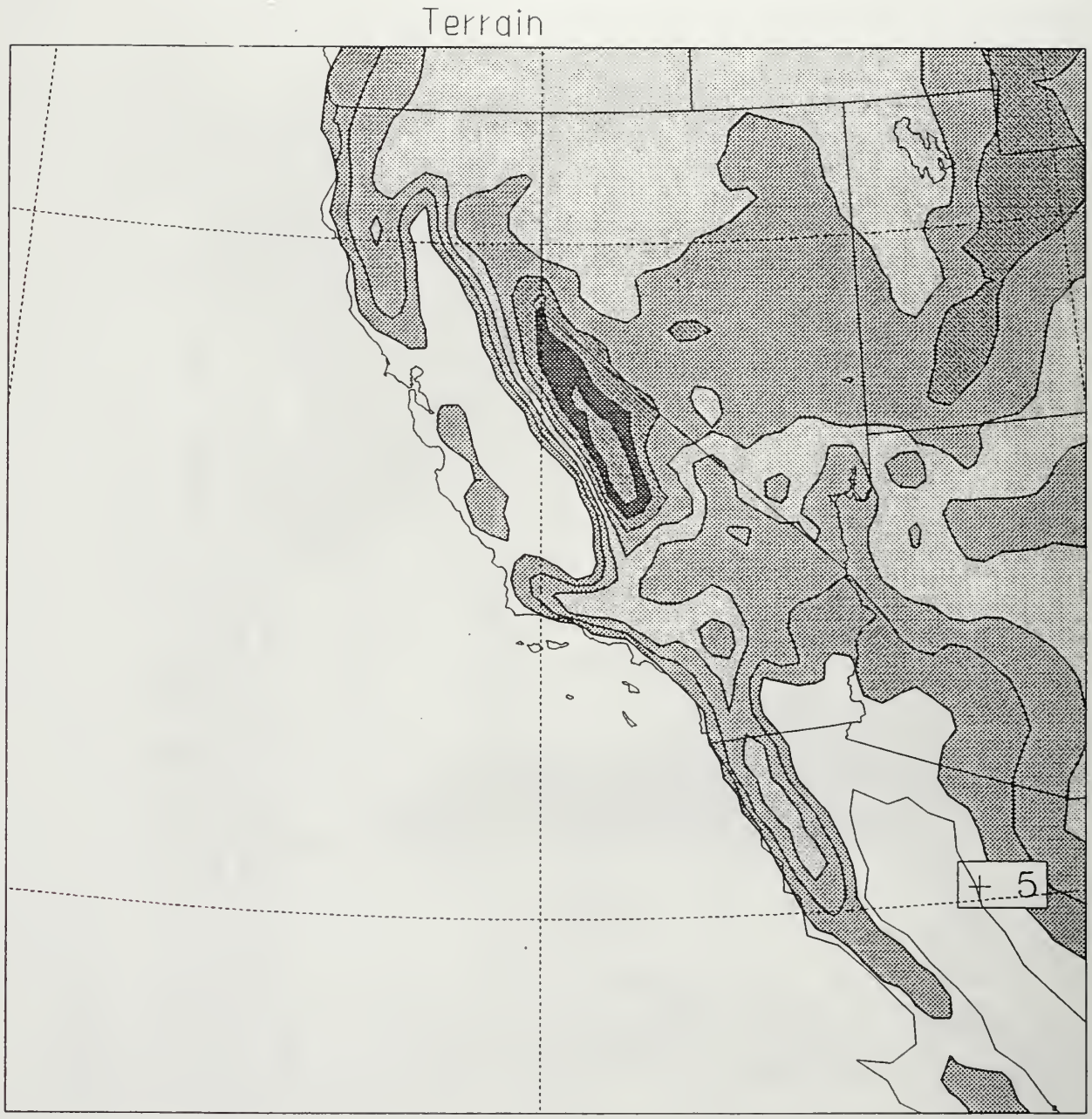

Fig. 6. The terrain field at the inner 27 km resolution domain used for the COAMPS model run, shaded at 500 m increments starting at 500 m.

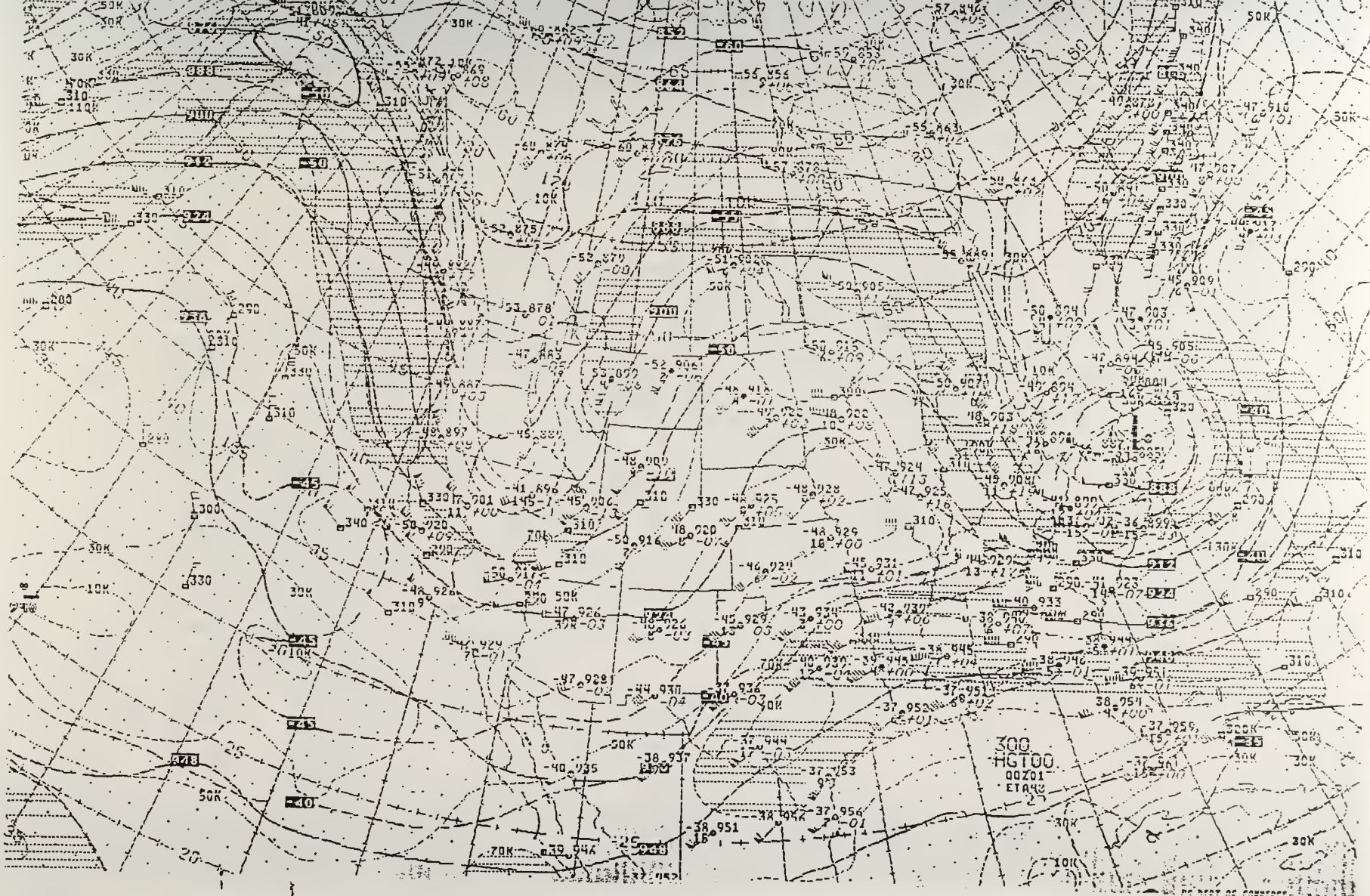

Fig. 7. NCEP difax 300 mb chart for 0000 UTC 1 April 1997. Height contours are solid lines (12 dm increment) and isotherms are heavy dashed lines (5° C increment). Isotachs are thin dashed lines (20 kt increment) and are shaded every 40 kt beginning at 70 kt.

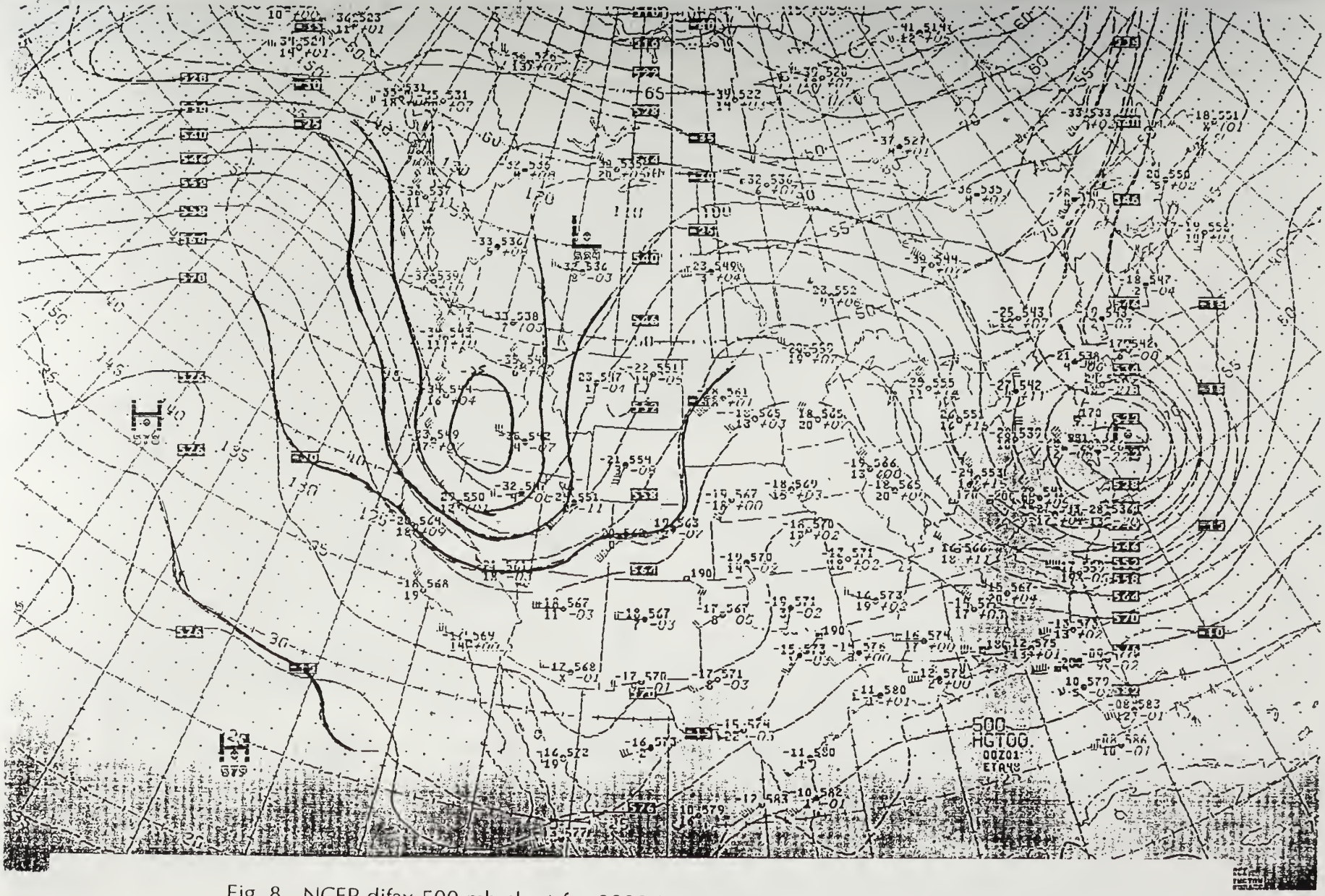

Fig. 8. NCEP difax 500 mb chart for 0000 UTC 1 April 1997. Height contours are solid lines (6 dm increment) and isotherms are dashed (5° C increment).

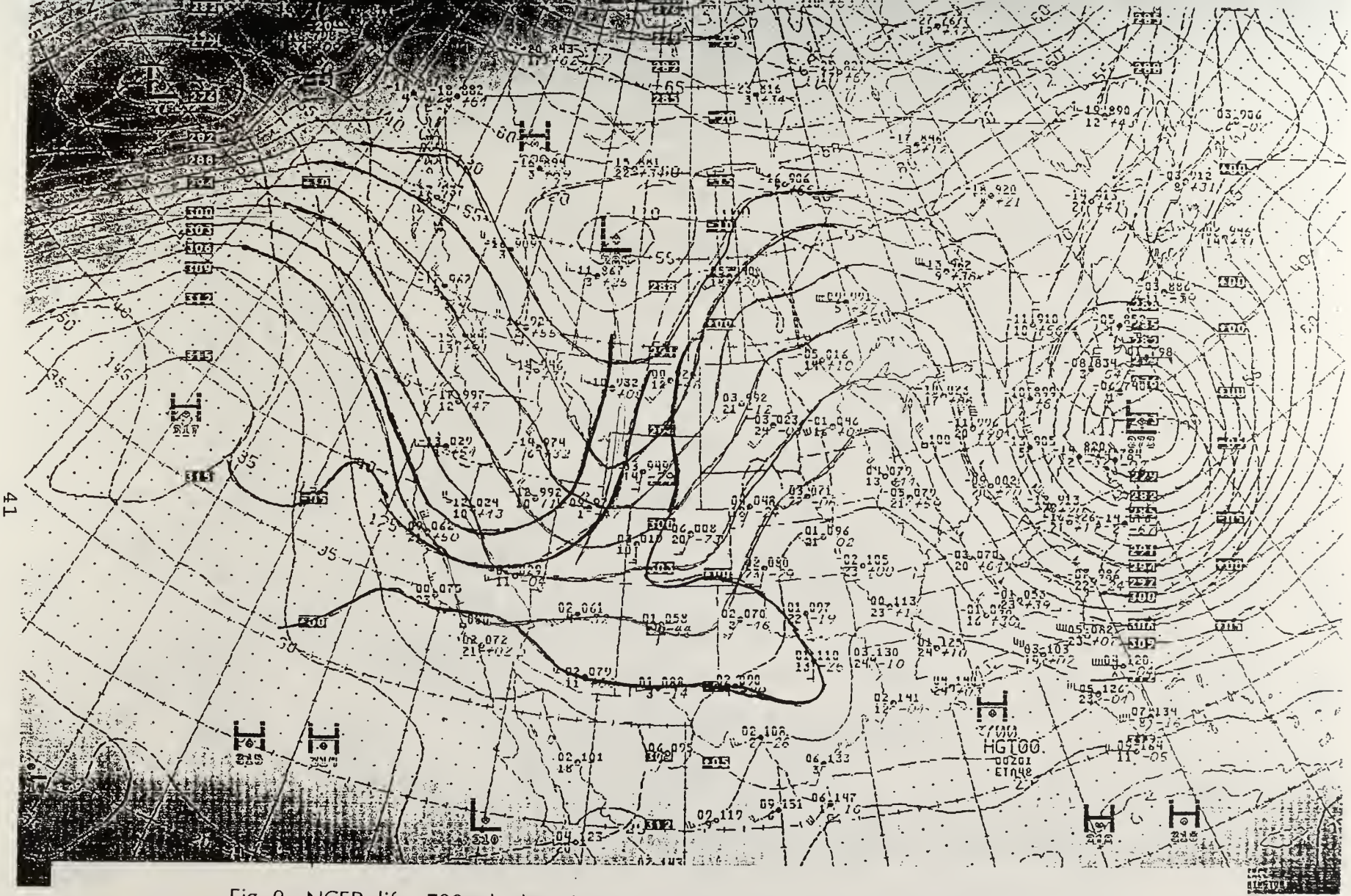

Fig. 9. NCEP difax 700 mb chart for 0000 UTC 1 April 1997. Height contours are solid lines (3 dm increment) and isotherms are dashed (5° C increment).

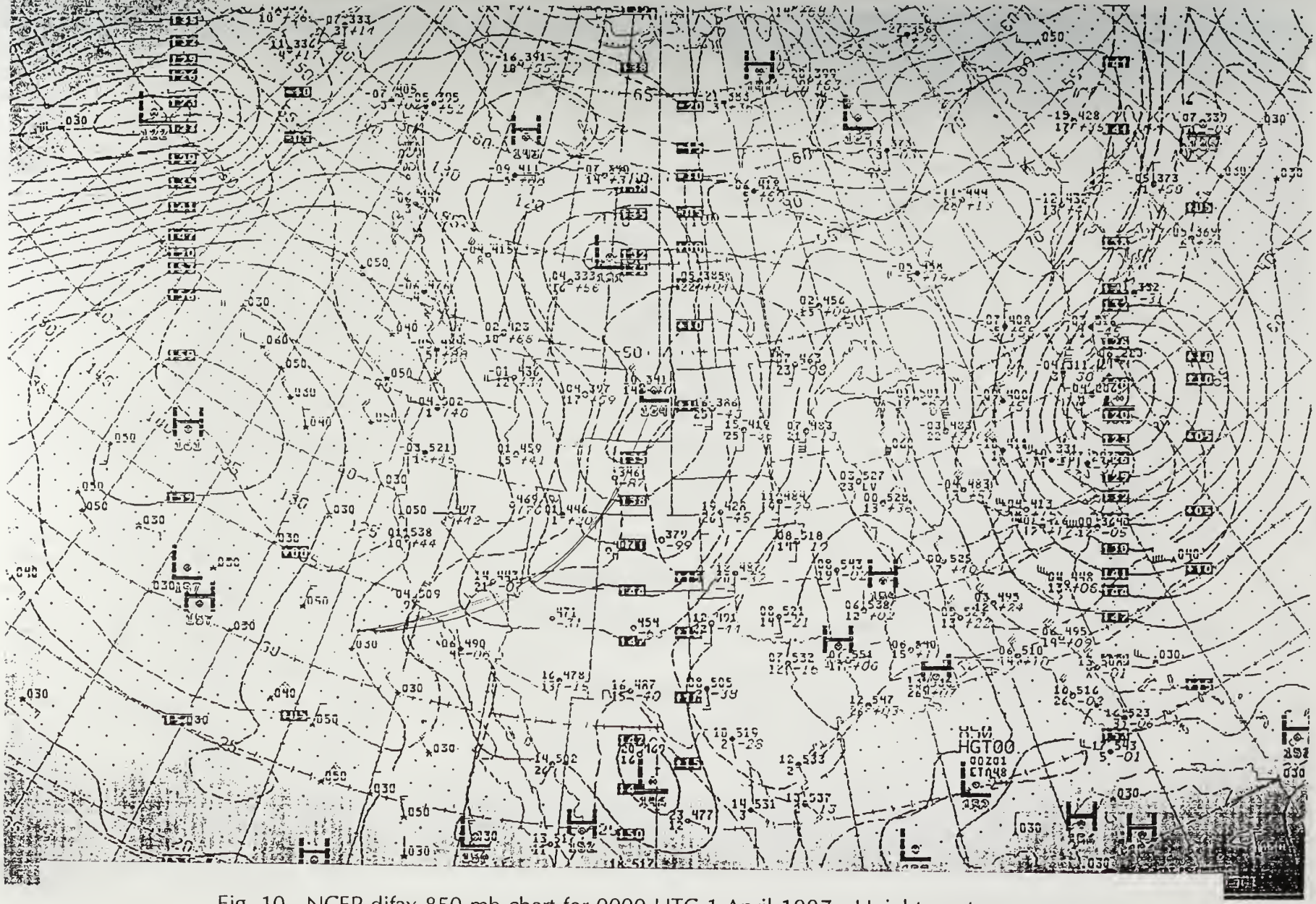

Fig. 10. NCEP difax 850 mb chart for 0000 UTC 1 April 1997. Height contours are solid lines (3 dm increment) and isotherms are dashed (5° C increment).

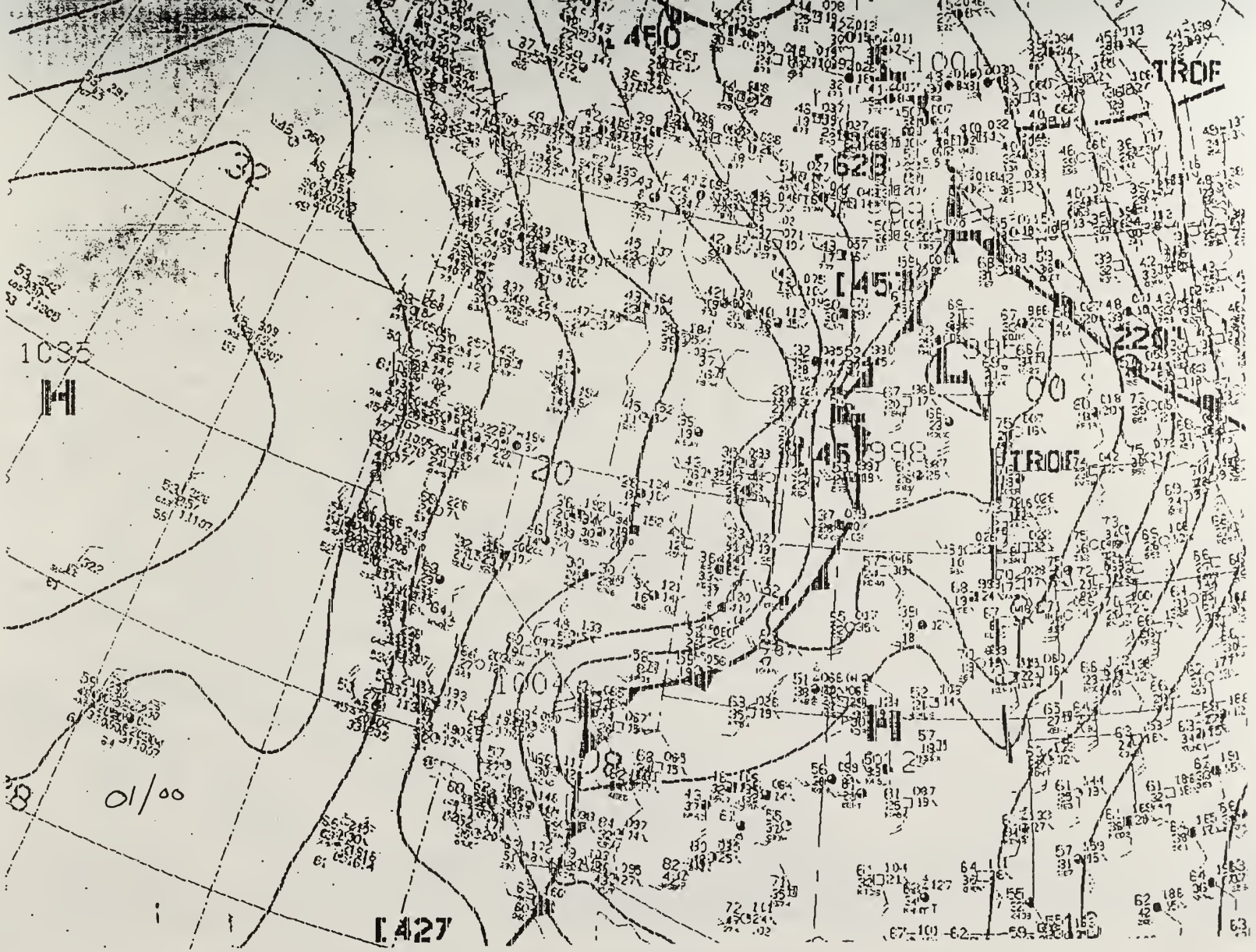

Fig. 11. NCEP difax surface chart for 0000 UTC 1 April 1997. Isobars are solid lines (4 mb increment). Highs (H), lows (L), and fronts as depicted using conventional symbols.

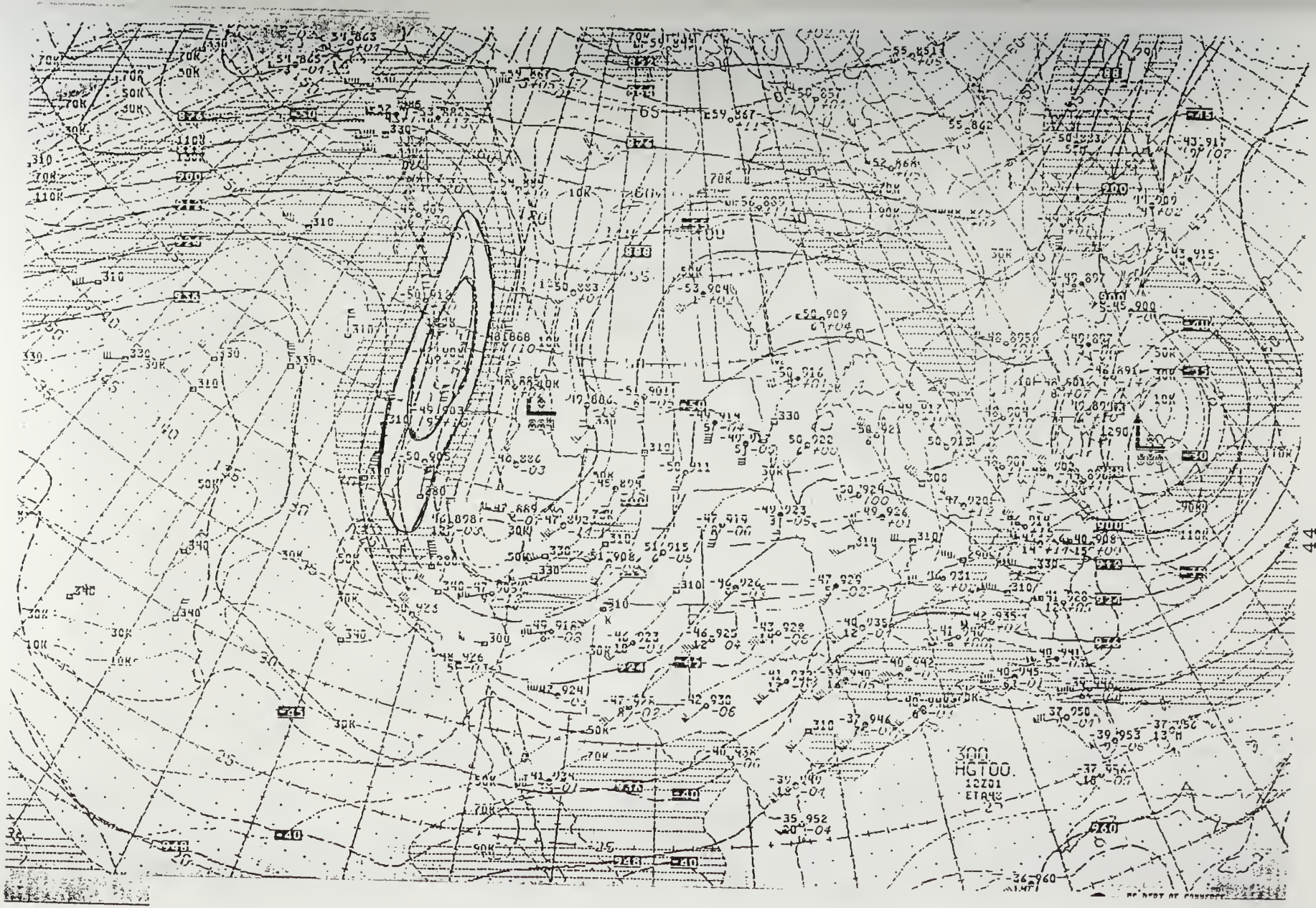

Fig. 12. Same as Fig. 7 but at 1200 UTC 1 April 1997.

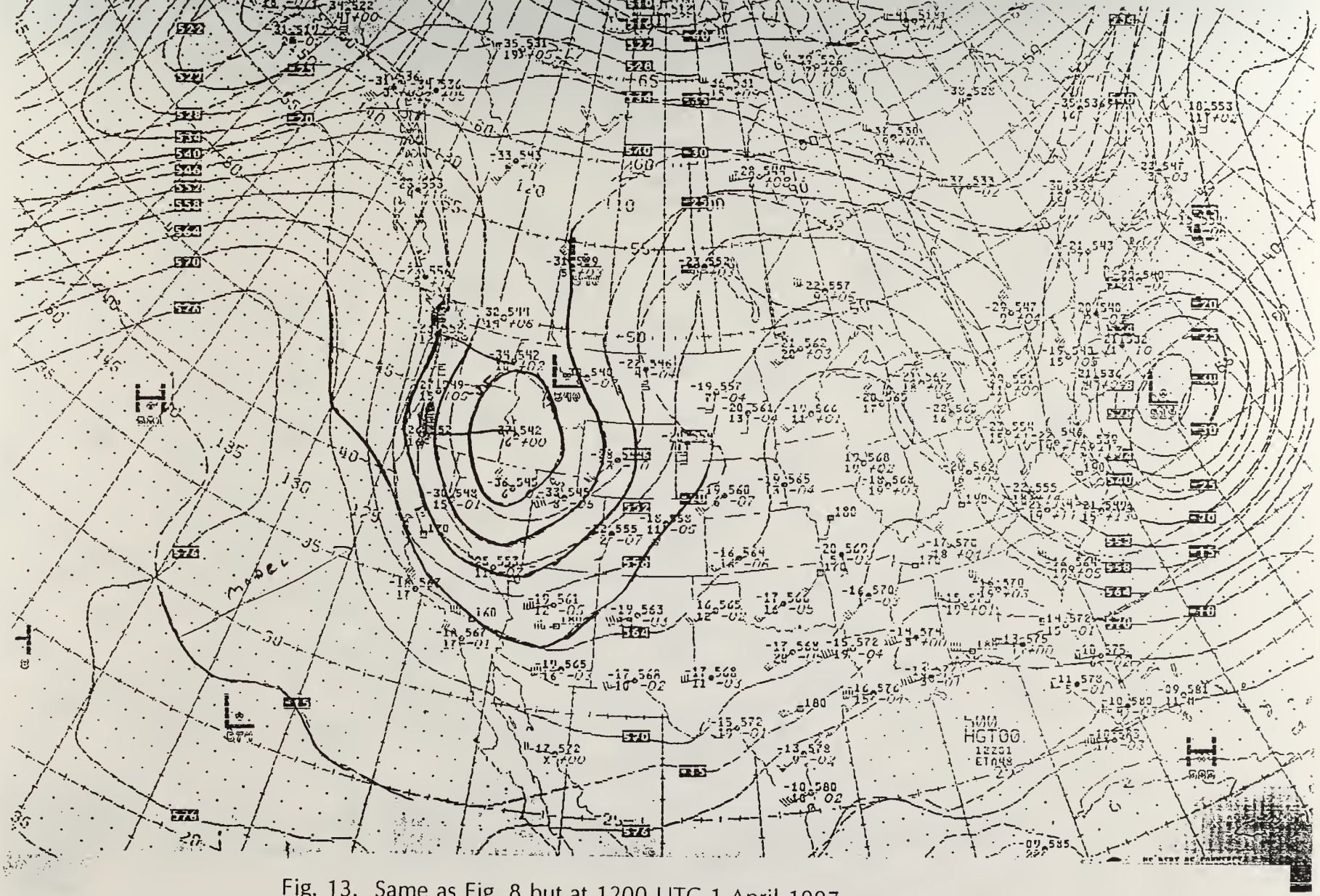

Fig. 13. Same as Fig. 8 but at 1200 UTC 1 April 1997.

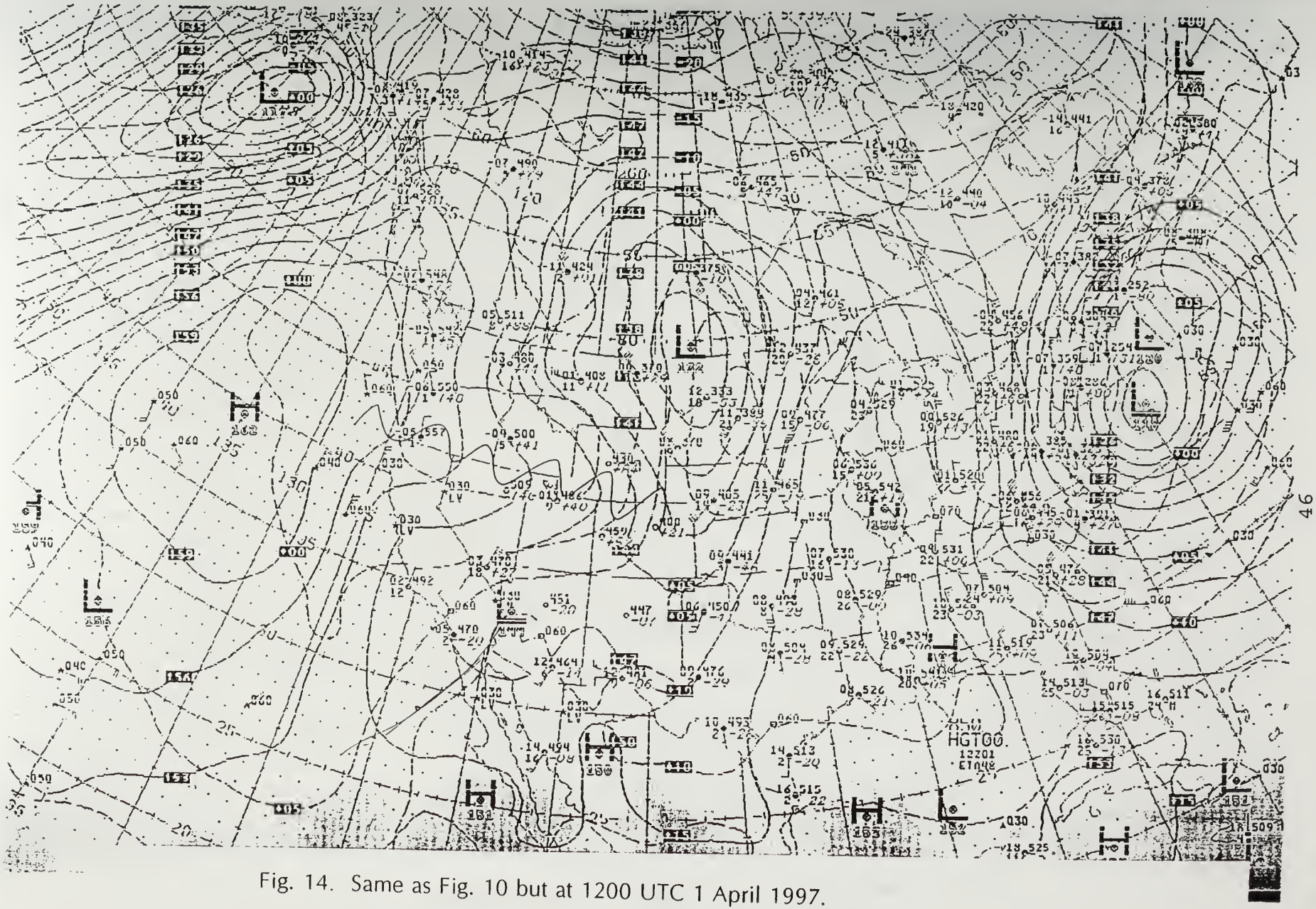

Fig. 14. Same as Fig. 10 but at 1200 UTC 1 April 1997.

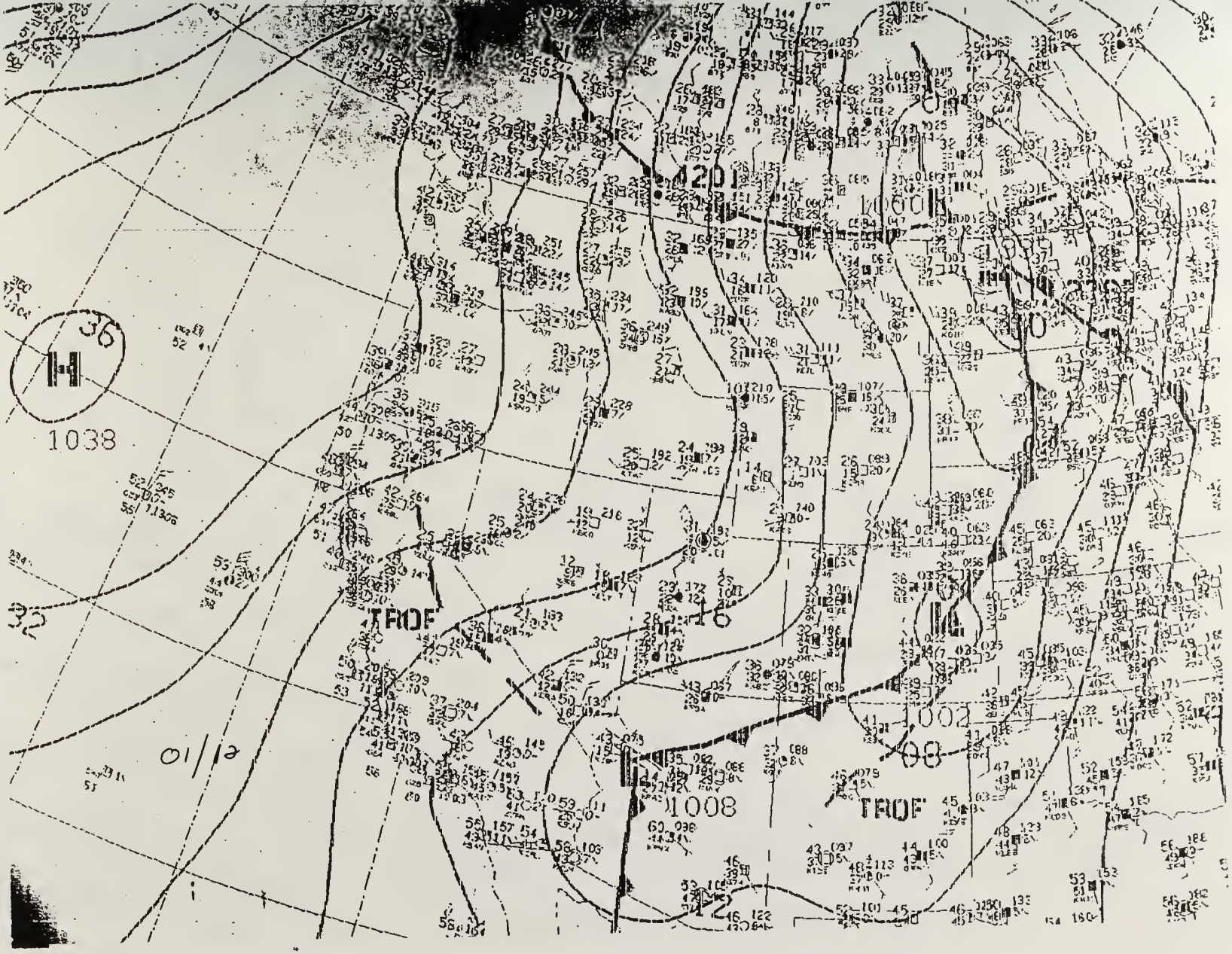

Fig. 15. Same as Fig. 11 but at 1200 UTC 1 April 1997.

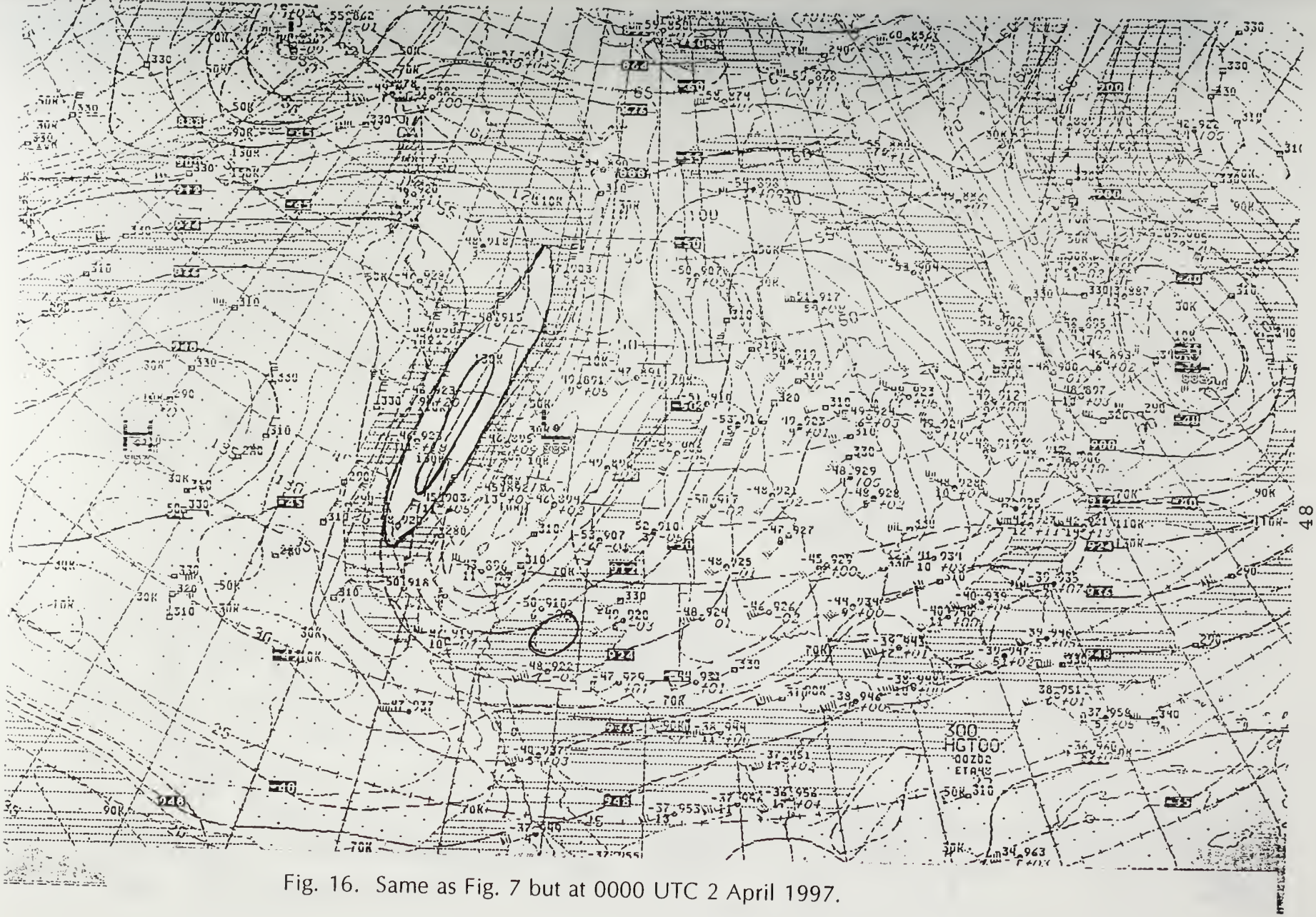

Fig. 16. Same as Fig. 7 but at 0000 UTC 2 April 1997.

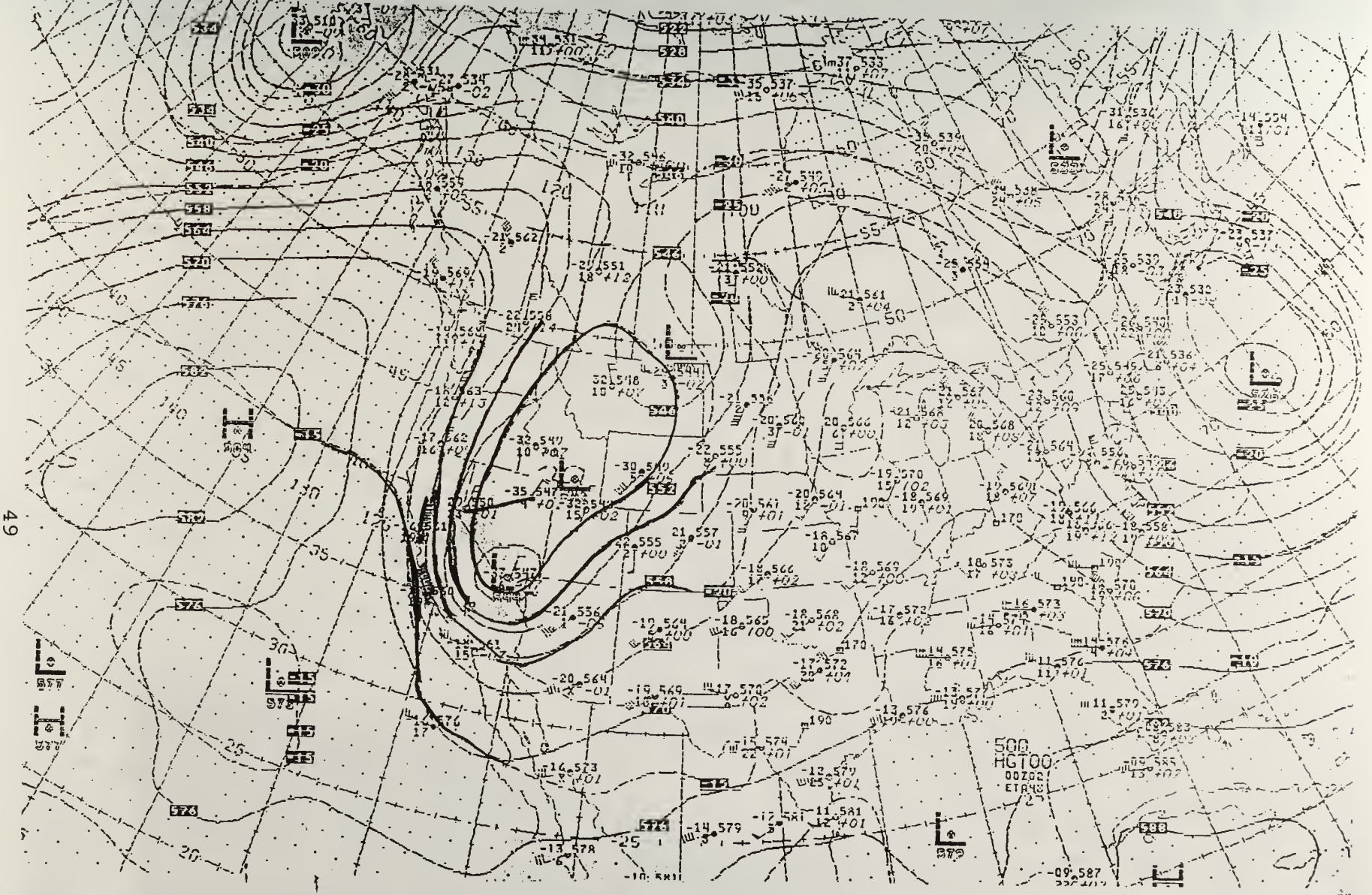

Fig. 17. Same as Fig. 8 but at 0000 UTC 2 April 1997.

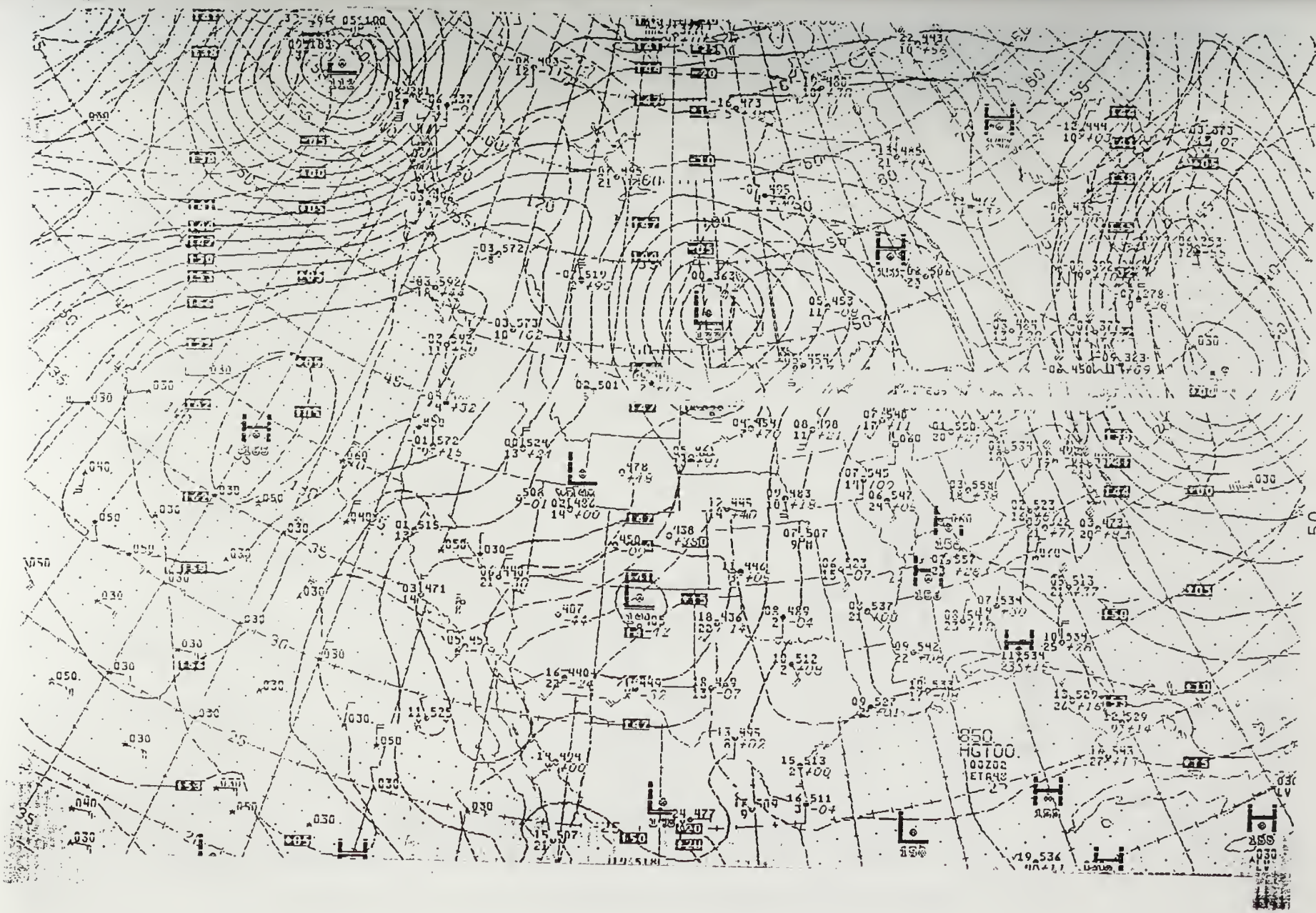

Fig. 18. Same as Fig. 10 but at 0000 UTC 2 April 1997.

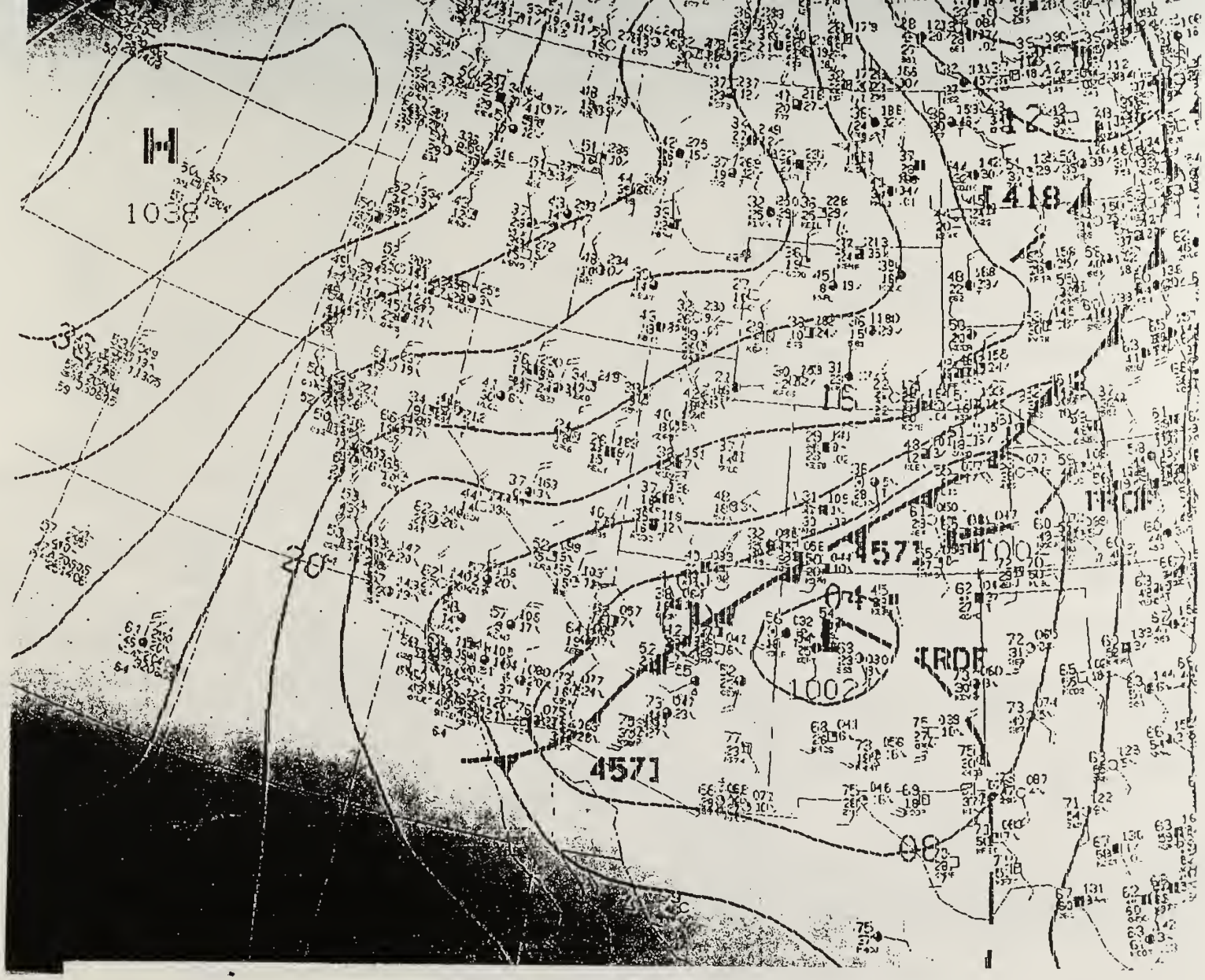

Fig. 19. Same as Fig. 11 but at 0000 UTC 2 April 1997.

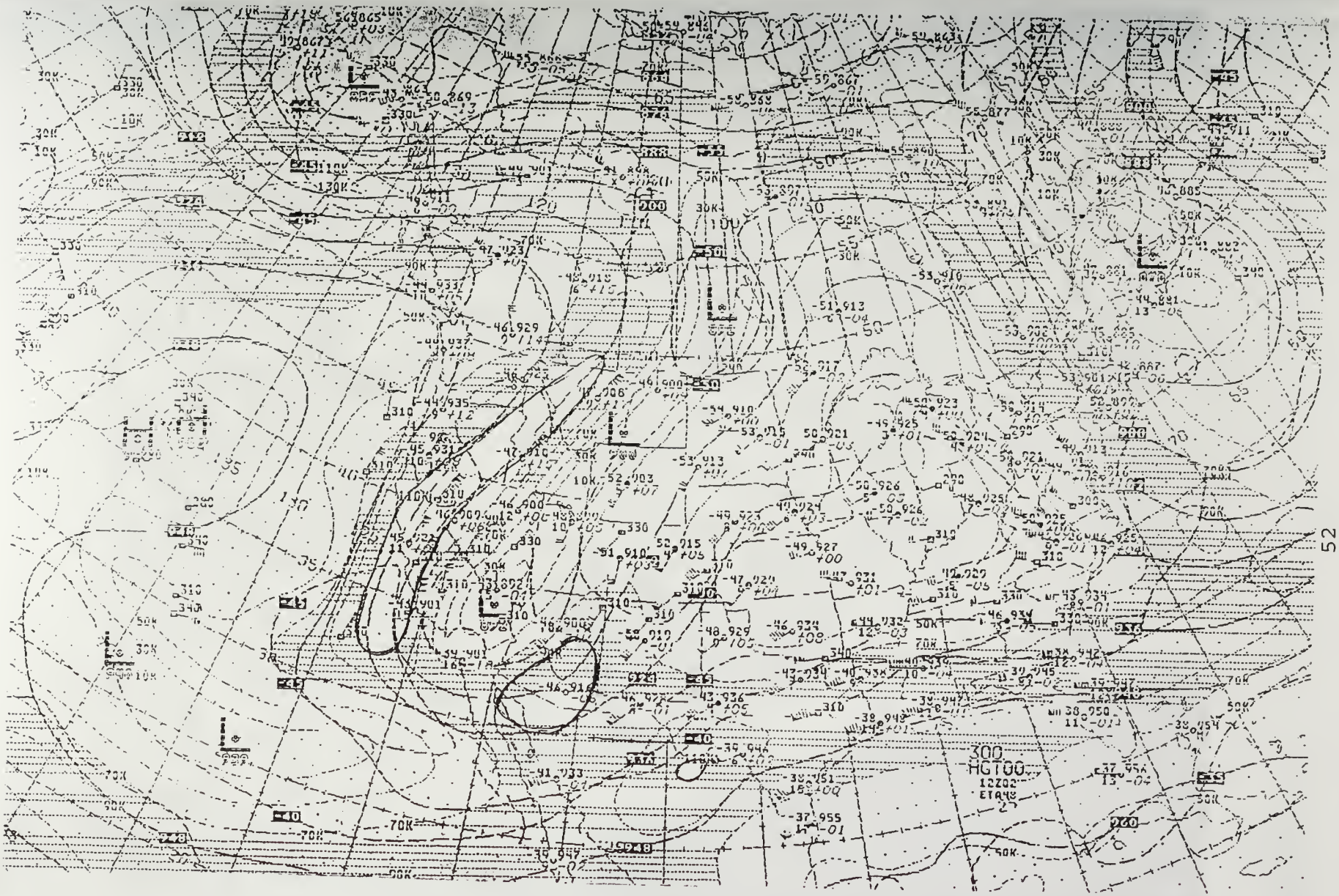

Fig. 20. Same as Fig. 7 but at 1200 UTC 2 April 1997.

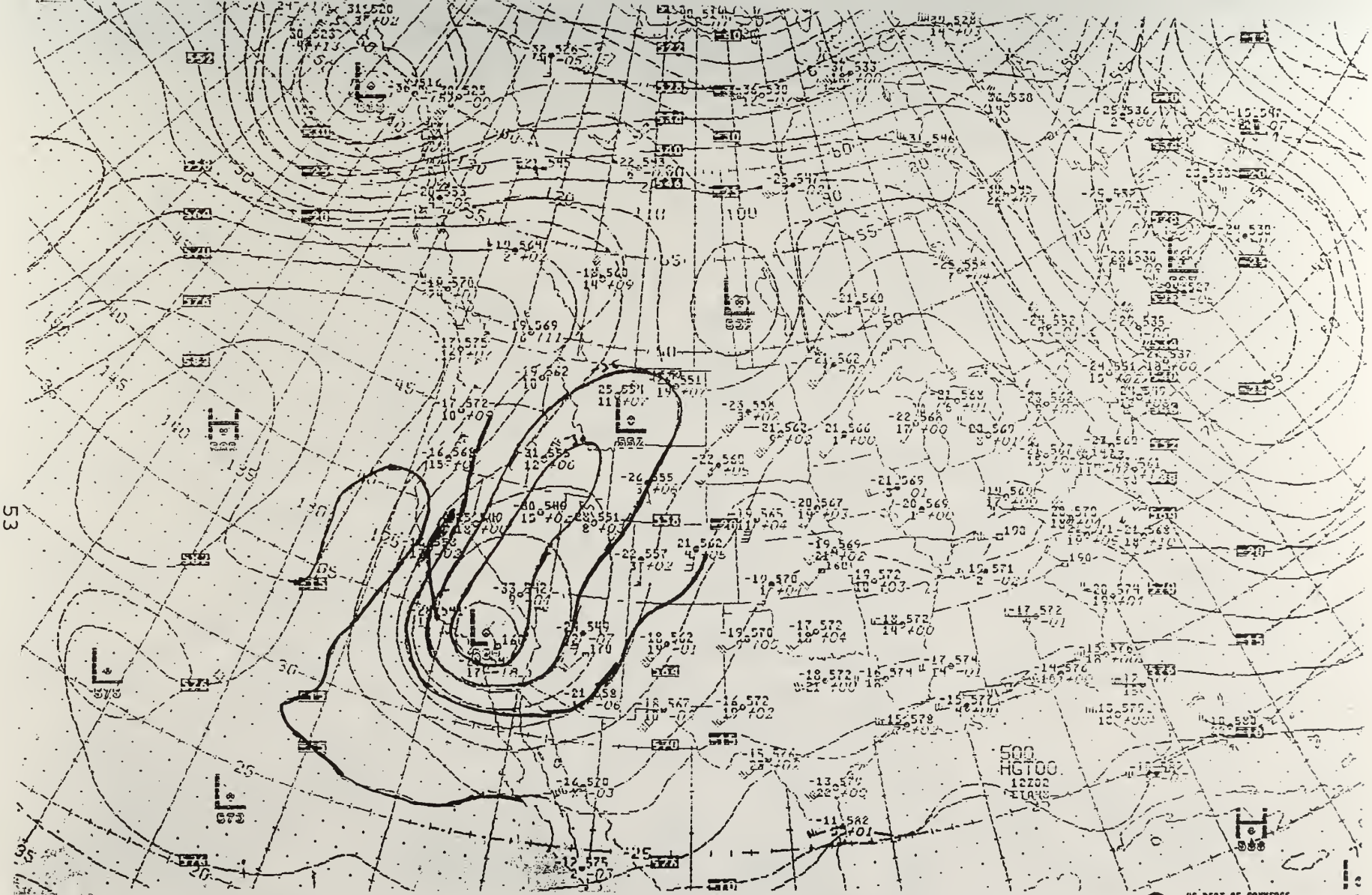

Fig. 21. Same as Fig. 8 but at 1200 UTC 2 April 1997.

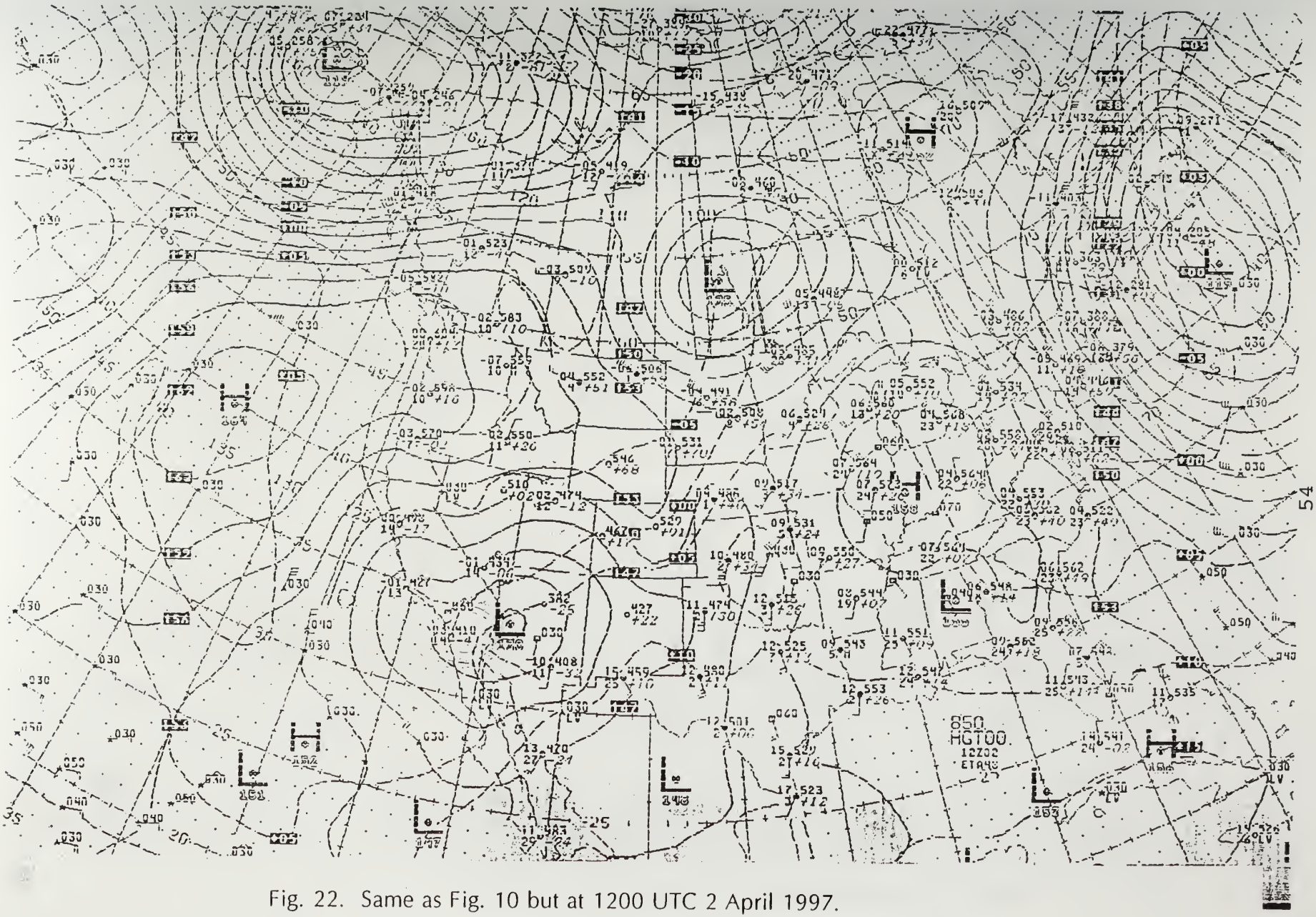

Fig. 22. Same as Fig. 10 but at 1200 UTC 2 April 1997.

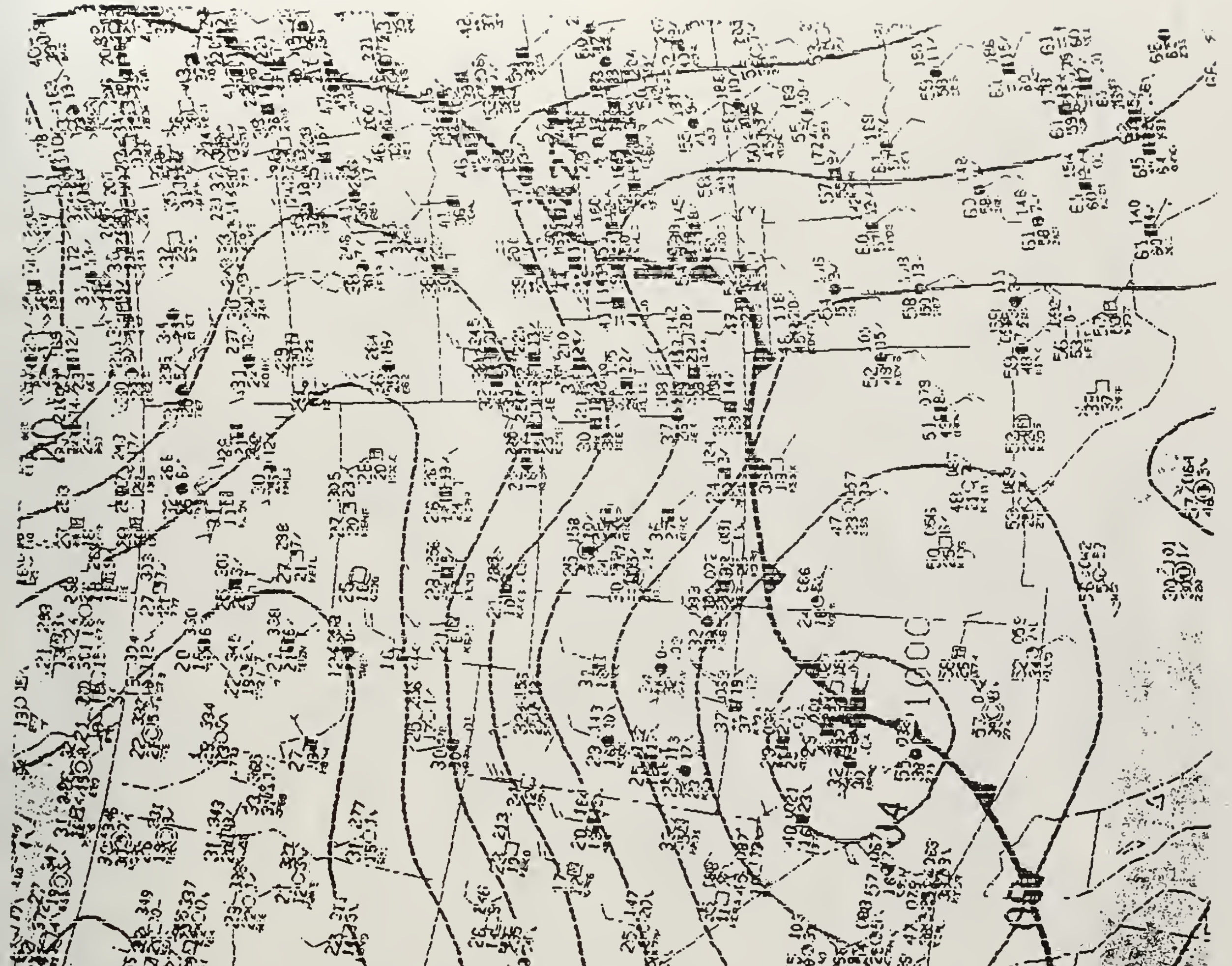

Fig. 23. Same as Fig. 11 but at 1200 UTC 2 April 1997.

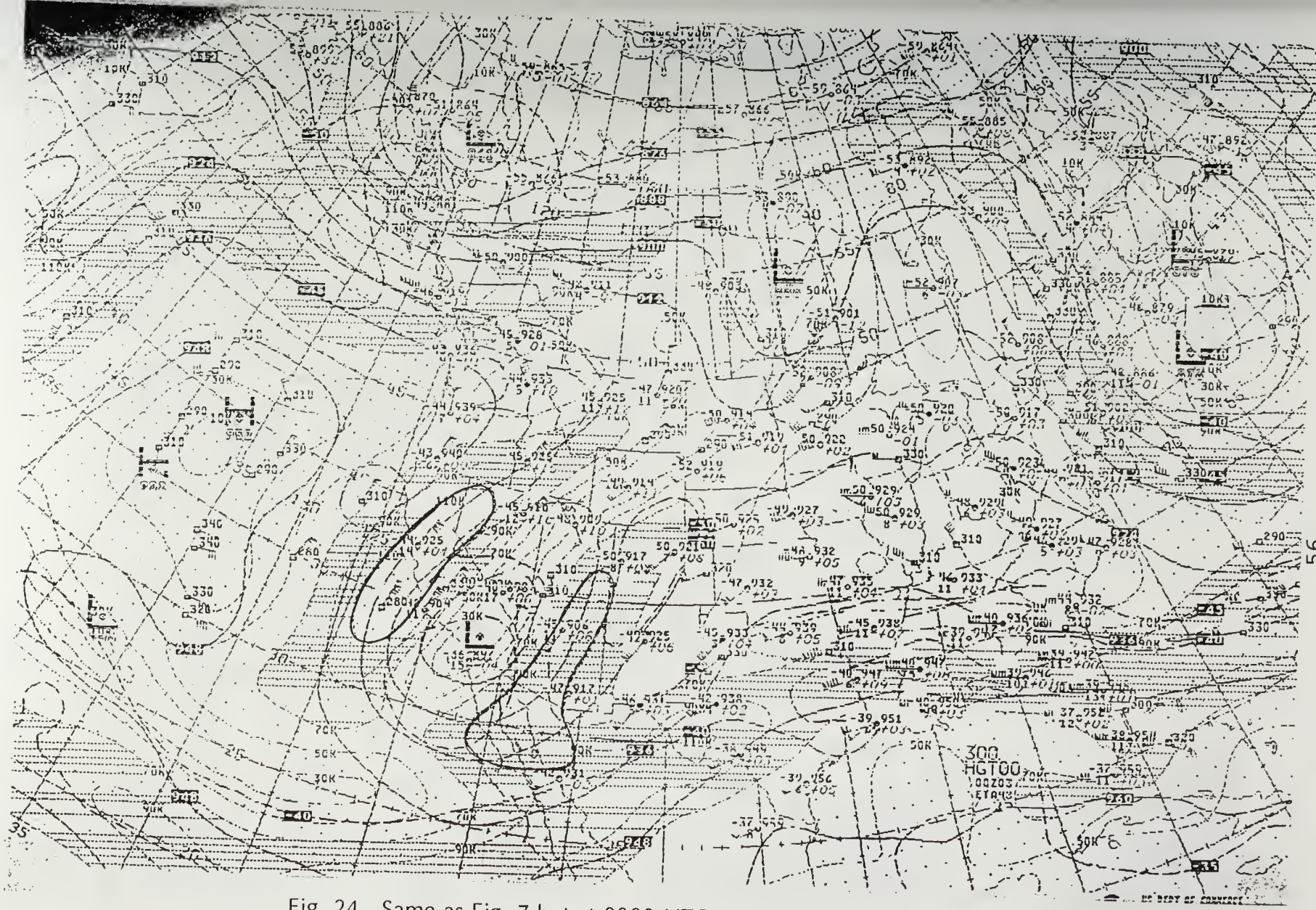

Fig. 24. Same as Fig. 7 but at 0000 UTC 3 April 1997.

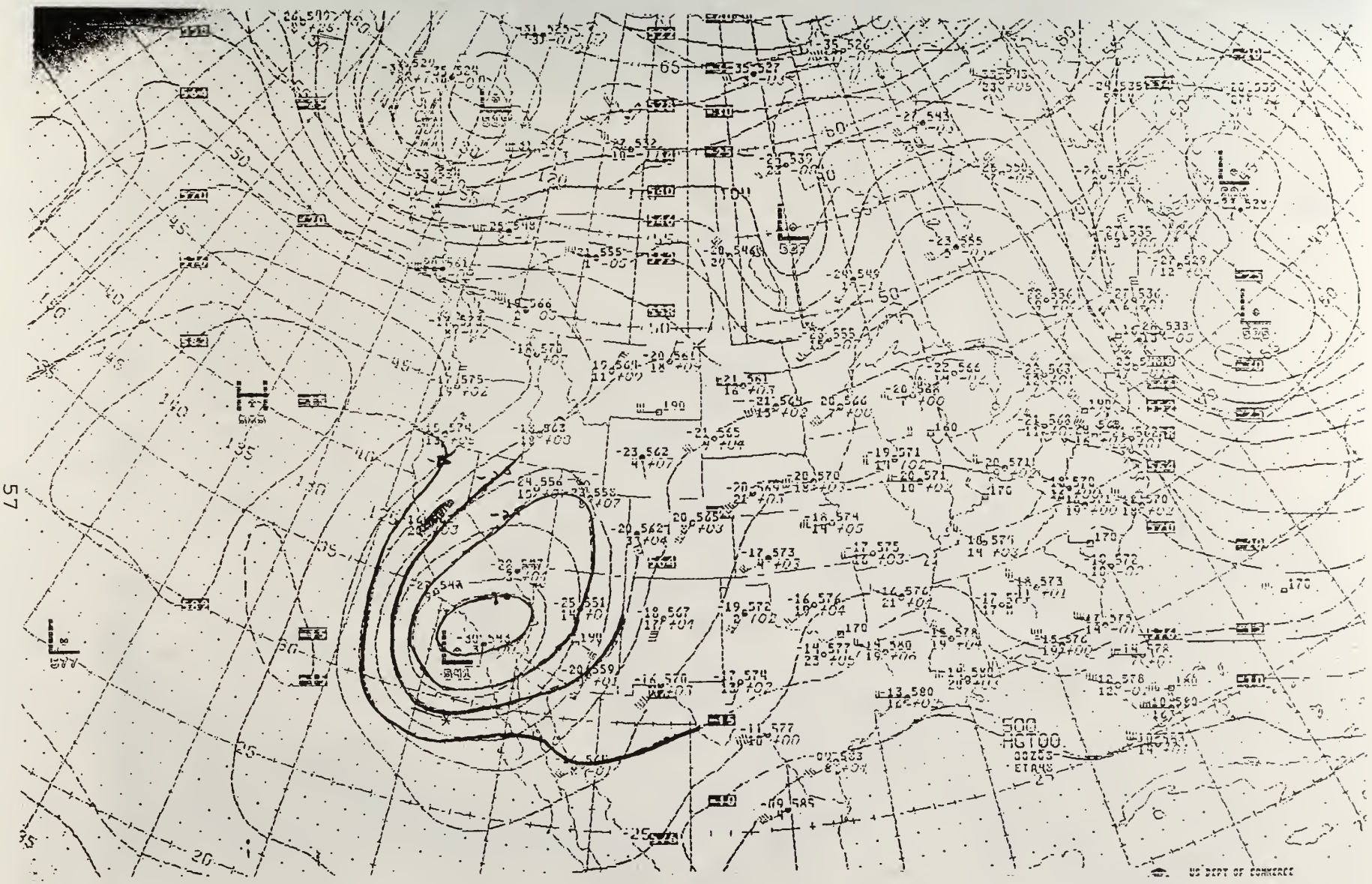

Fig. 25. Same as Fig. 8 but at 0000 UTC 3 April 1997.

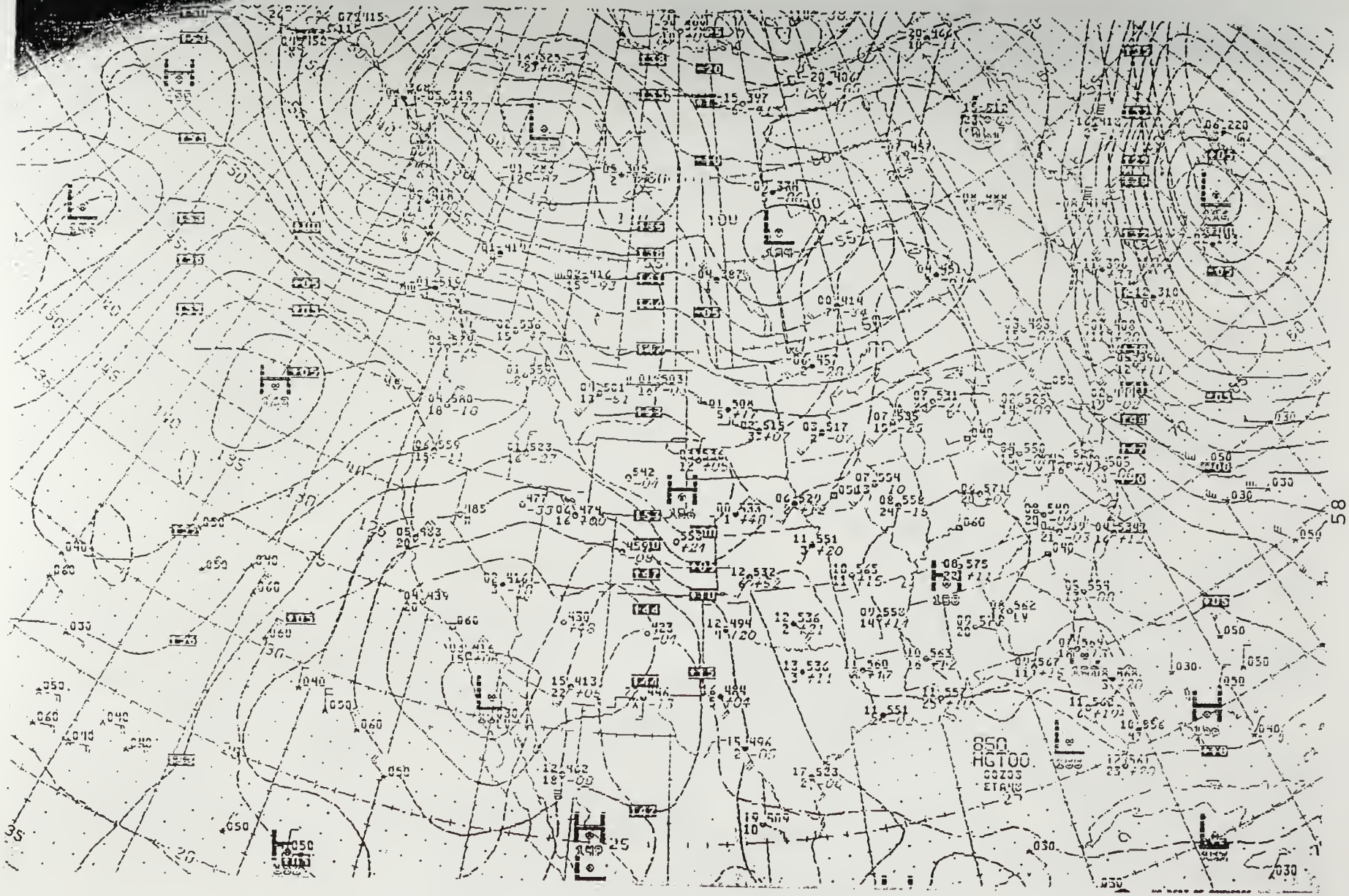

Fig. 26. Same as Fig. 10 but at 0000 UTC 3 April 1997.

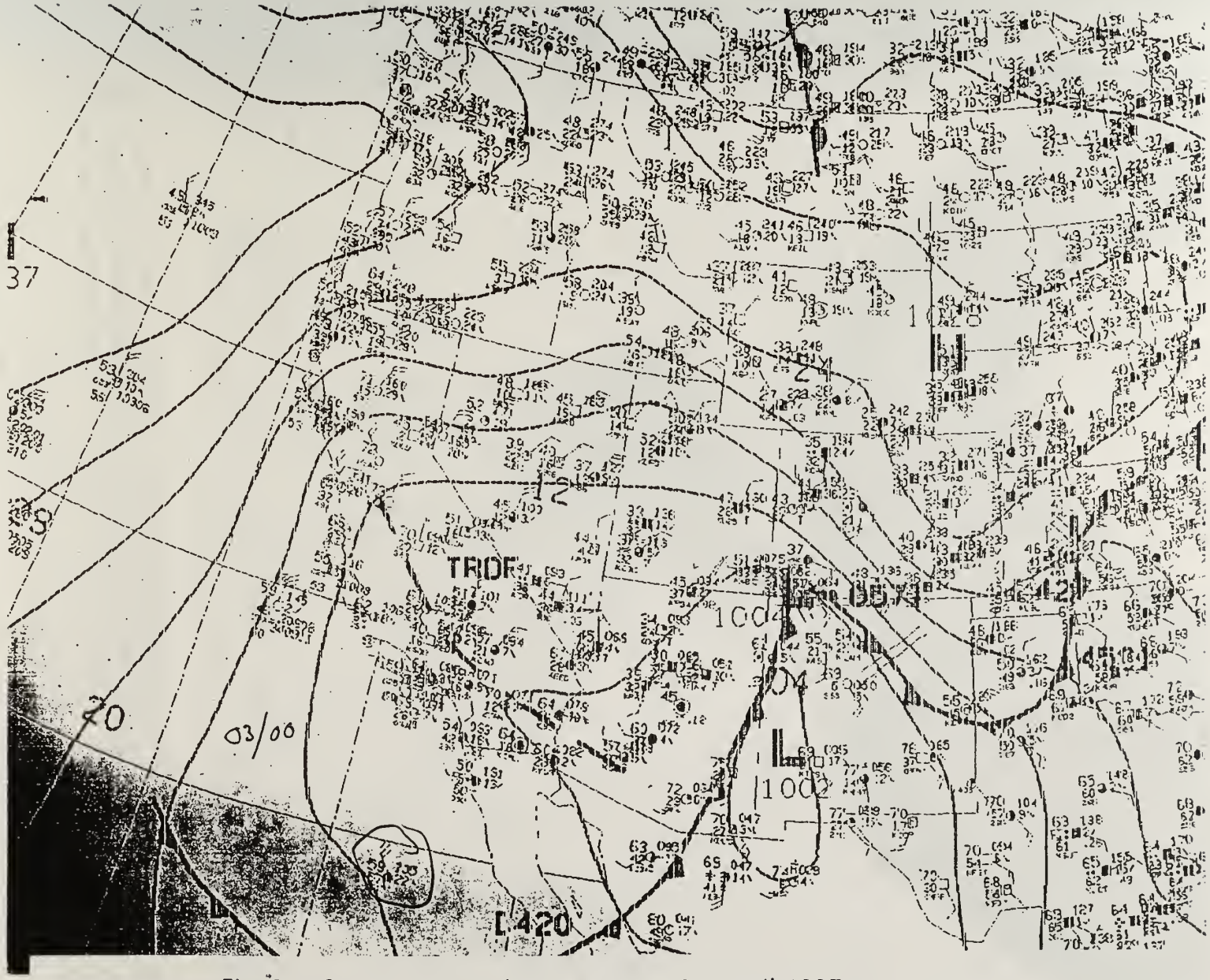

Fig. 27. Same as Fig. 11 but at 0000 UTC 3 April 1997.

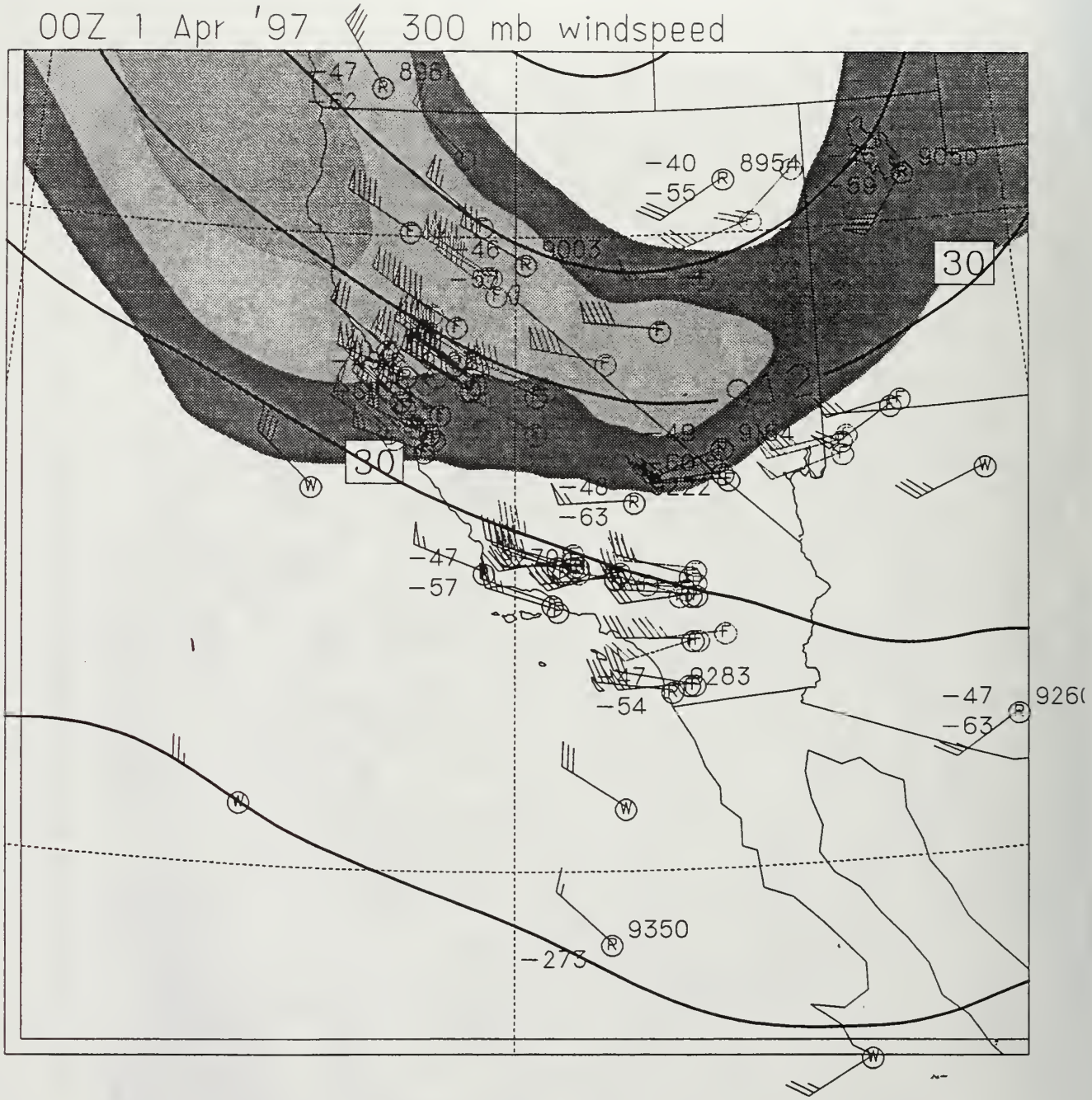

Fig. 28. COAMPS 300 mb chart at 0000 UTC 1 April 1997. Height contours are solid lines (12 dm increment), isotachs are shaded at 5 m/s increments starting at 30 m/s. Observations are in m/s: flag = 25 m/s, full barb = 5 m/s, and half barb = 2.5 m/s.

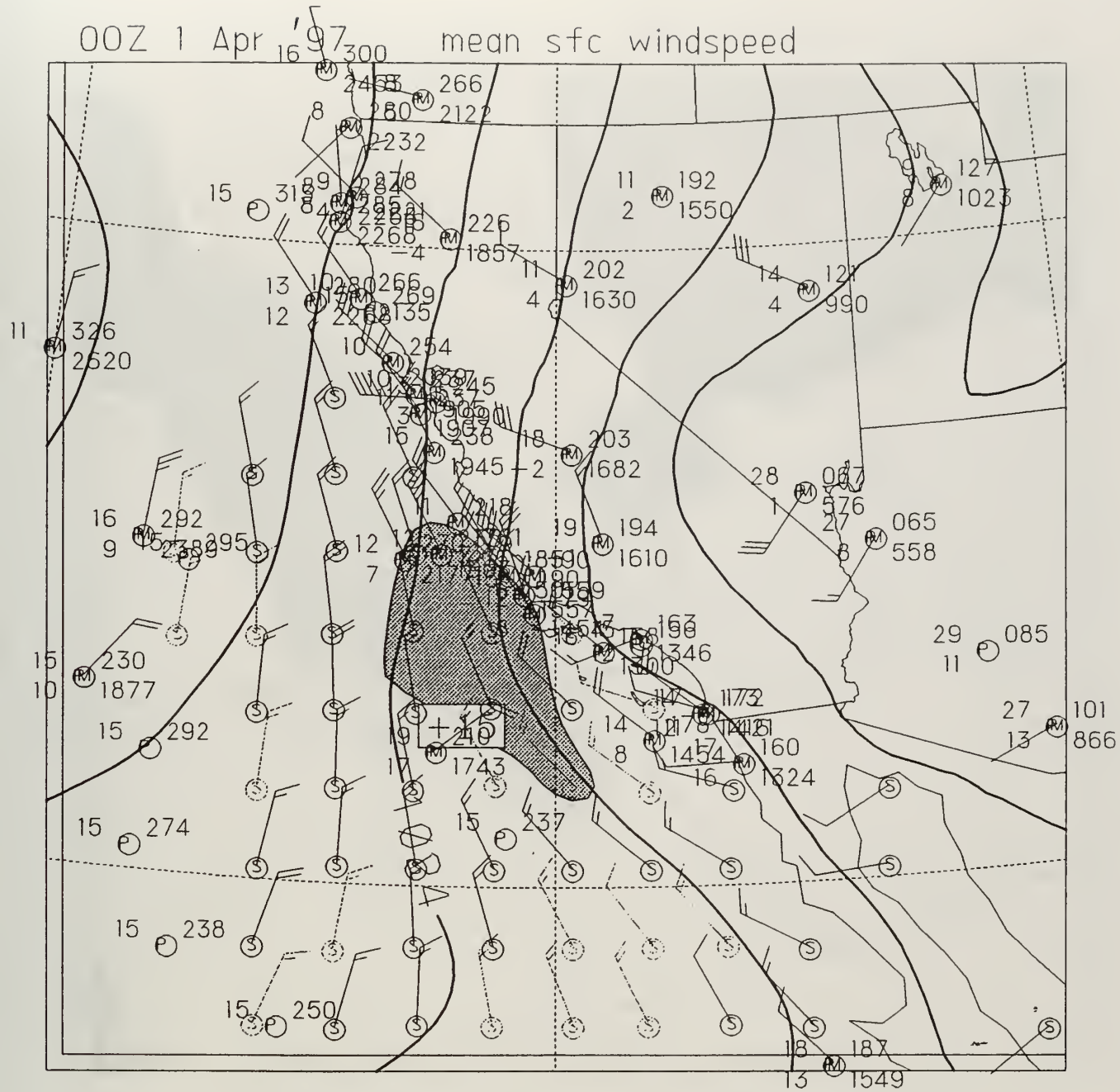

Fig. 29. COAMPS surface chart at 0000 UTC 1 April 1997. Isobars are solid lines (4 mb increment), isotachs of the average surface wind speed are shaded in 5 m/s increments starting at 15 m/s. Observations are in m/s: full barb = 5 m/s and half barb = 2.5 m/s. The average windspeed here is defined as the average of the lowest four sigma levels, corresponding to the lowest 90 m. Values are weighted by the layer depth in forming the average.

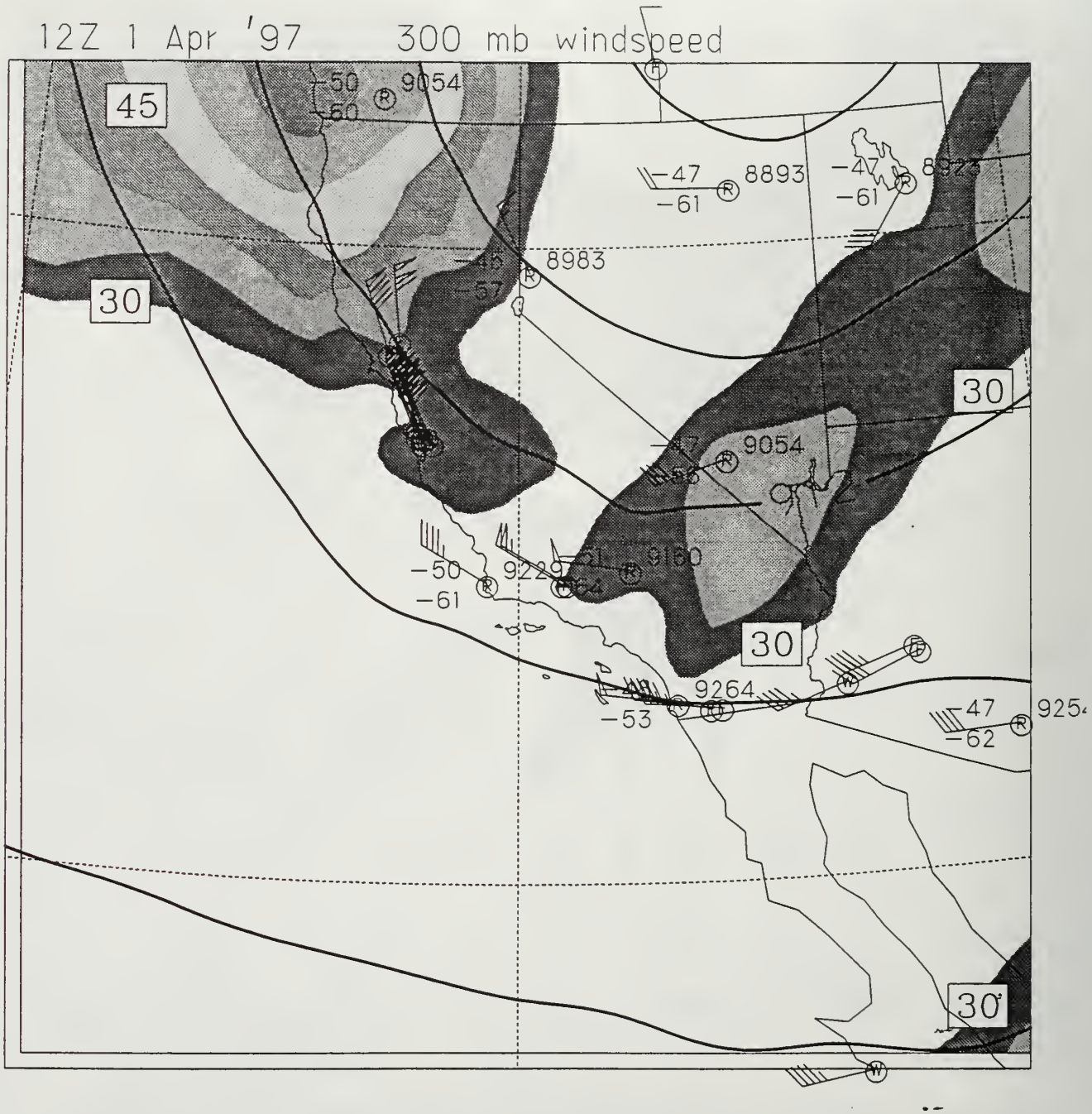

Fig. 30. Same as Fig. 28 except for 1200 UTC 1 April 1997.

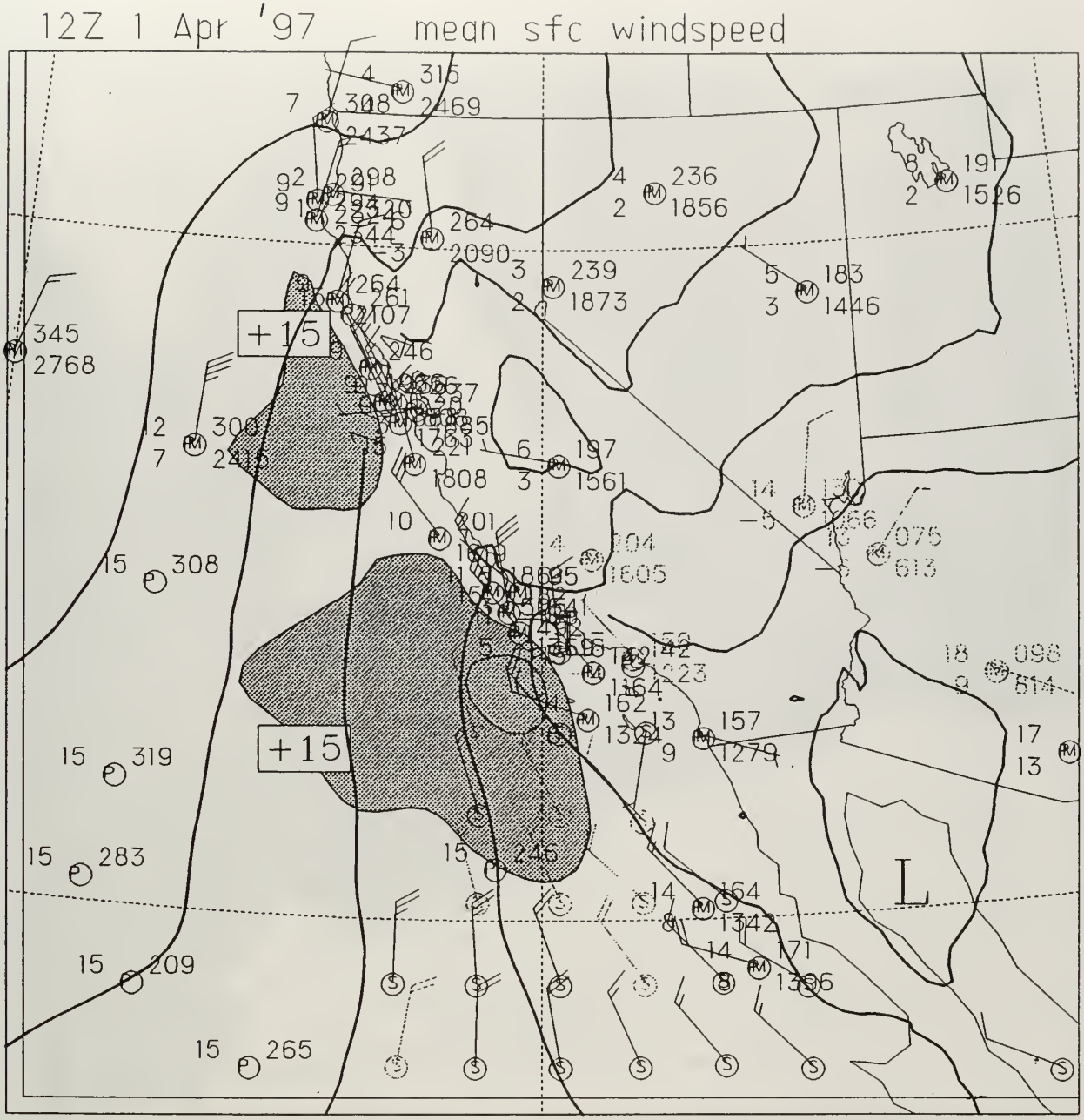

Fig. 31. Same as Fig. 29 except for 1200 UTC 1 April 1997. --

Fig. 32. Same as Fig. 28 except for 0000 UTC 2 April 1997.

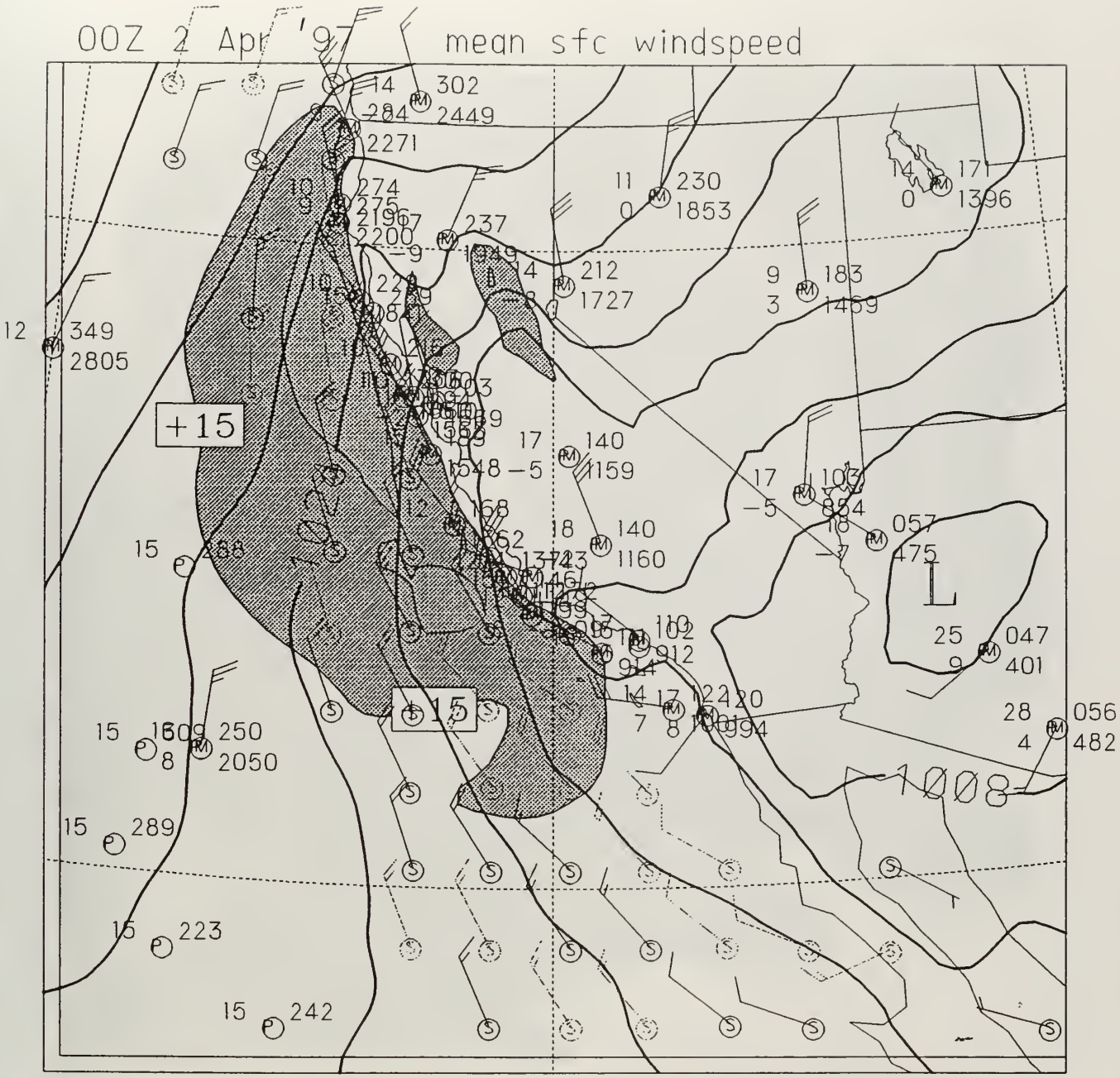

Fig. 33. Same as Fig. 29 except for 0000 UTC 2 April 1997.

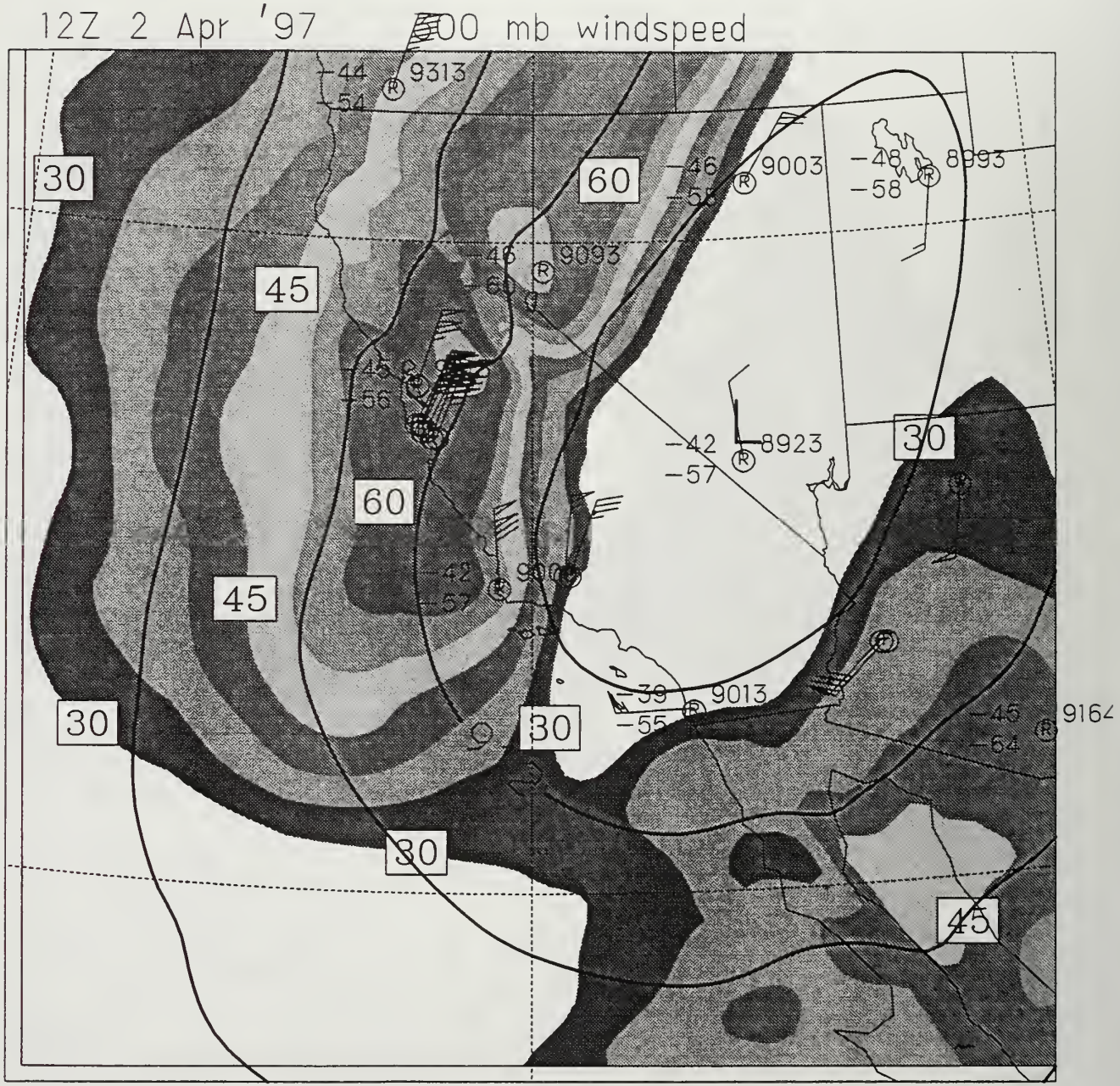

Fig. 34. Same as Fig. 28 except for 1200 UTC 2 April 1997.

Fig. 35. COAMPS 500 mb chart at 1200 UTC 2 April 1997. Height contours are solid lines (6 dm increment). Other fields as described in Fig. 28.

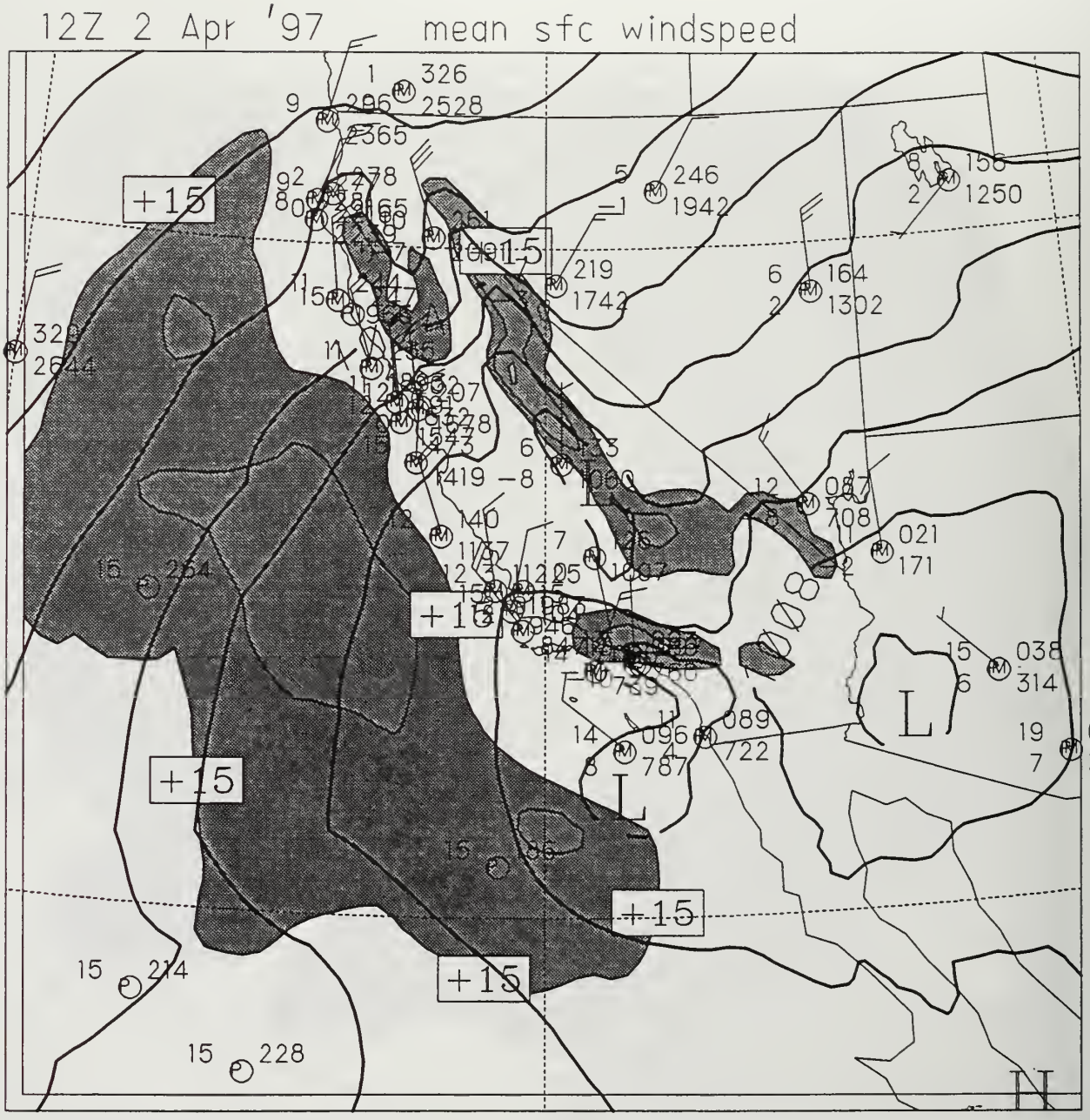

Fig. 36. Same as Fig. 29 except for 1200 UTC 2 April 1997.

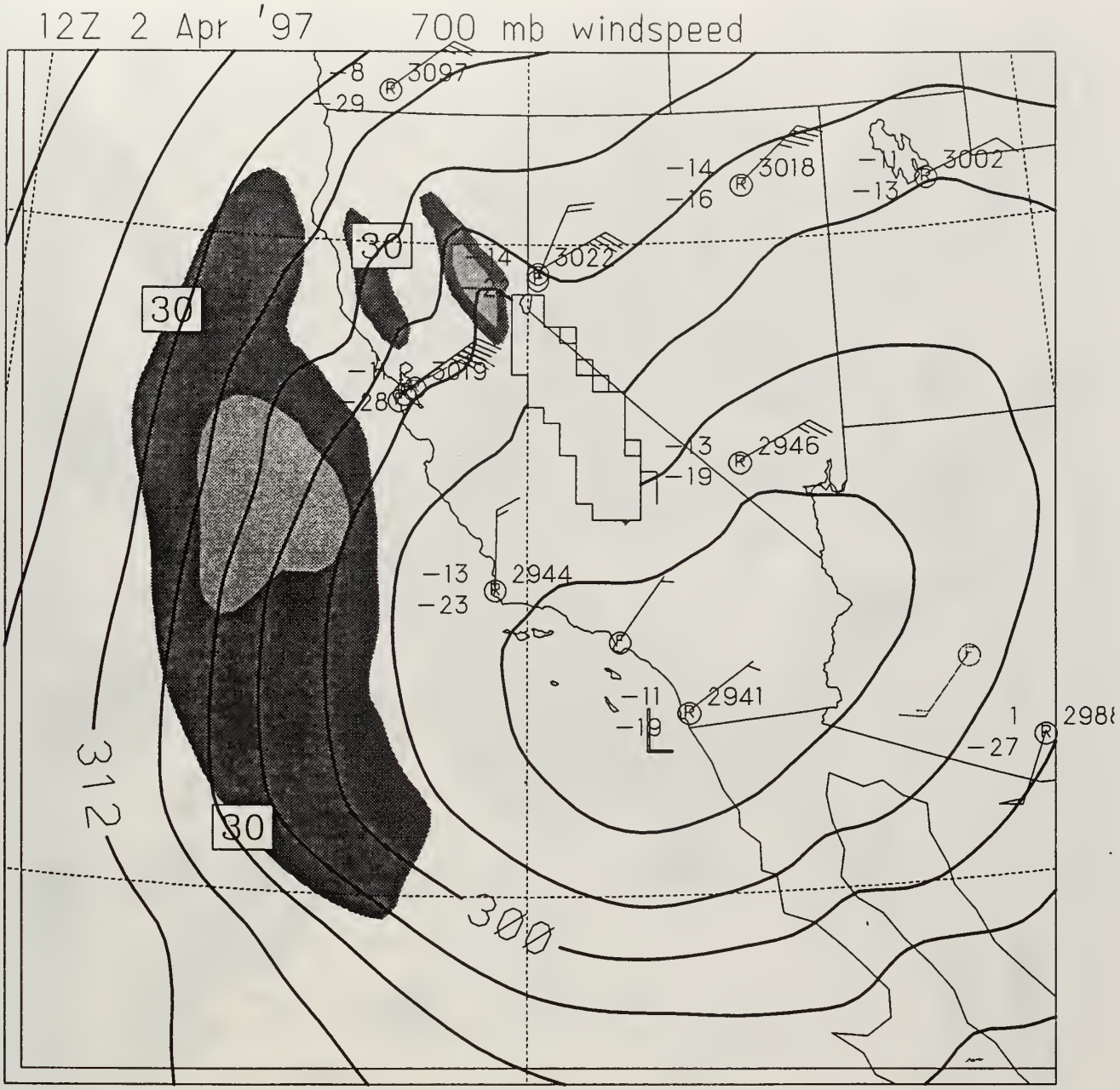

Fig. 37. COAMPS 700 mb chart at 1200 UTC 2 April 1997. Height contours are solid lines (3 dm increment). Other fields as described in Fig. 28.

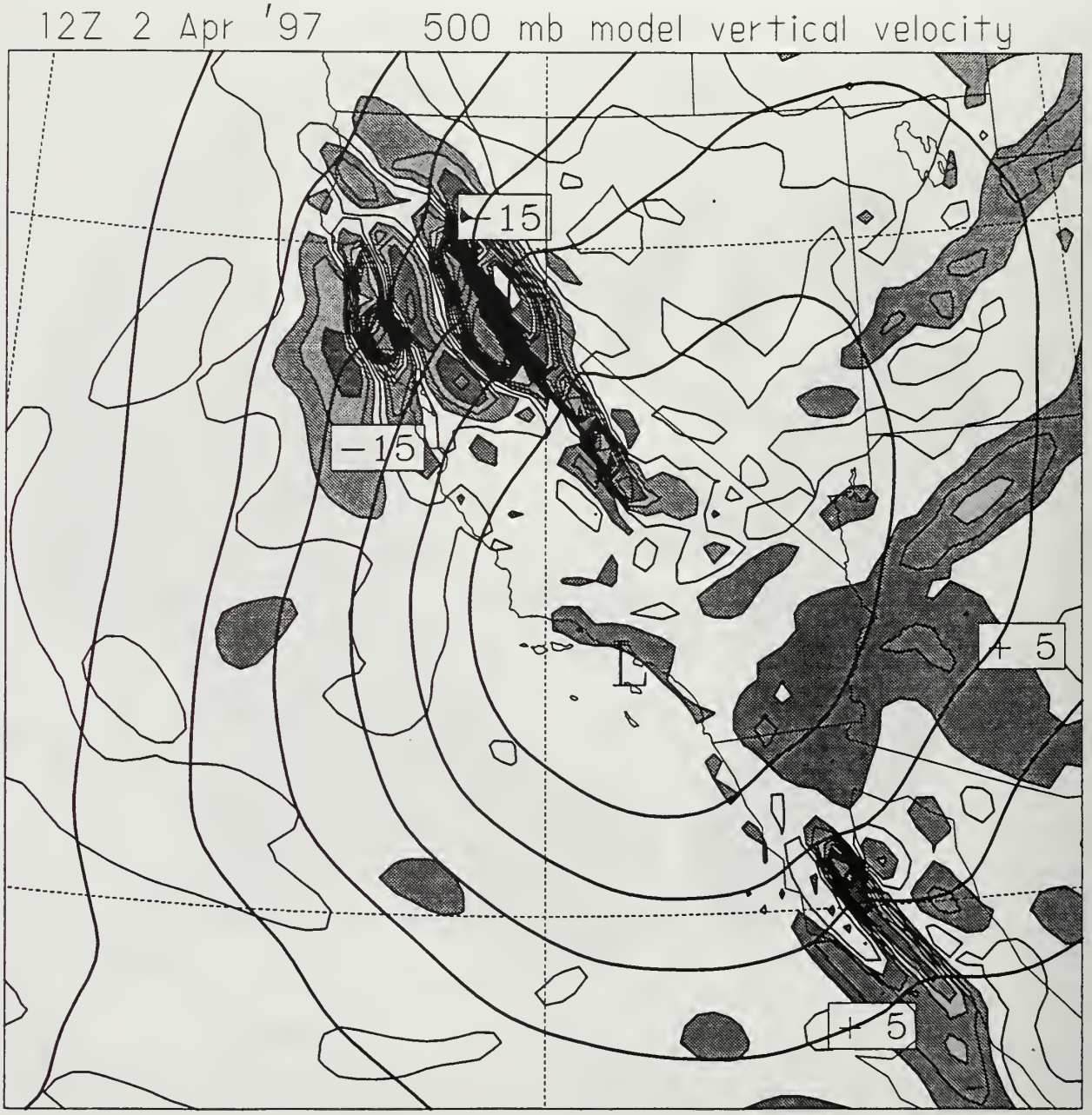

Fig. 38. COAMPS 500 mb chart at 1200 UTC 2 April 1997. Height contours are solid lines (6 dm increment). Vertical velocity field (w) is shaded in 10 cm/s increments beginning at 5 cm/s. Negative values indicate downward motion and positive values indicate upward motion.

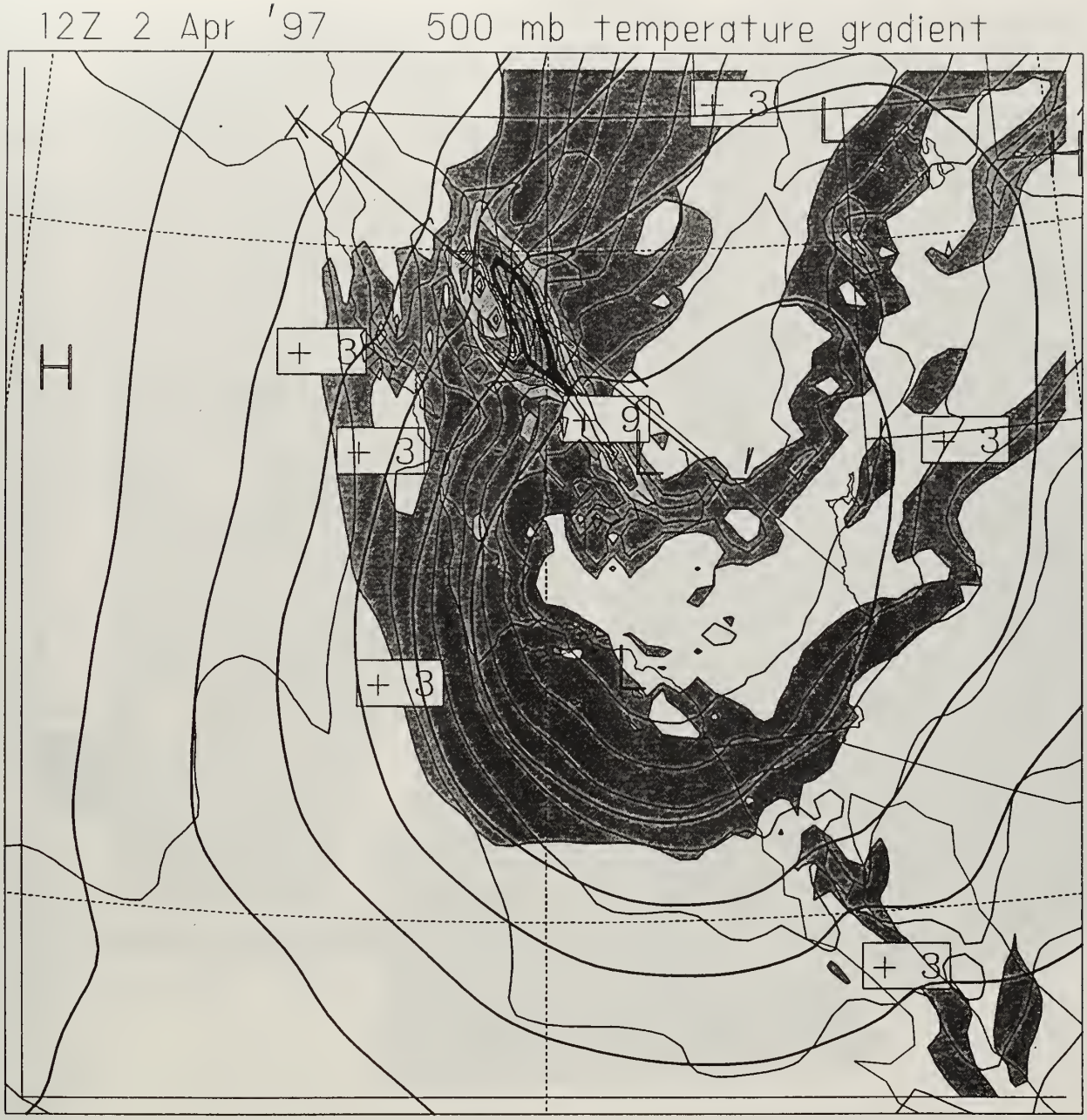

Fig. 39. COAMPS 500 mb chart at 1200 UTC 2 April 1997. Height contours are heavy solid lines (6 dm increment). Temperature is thin solid lines (2°C increment). Temperature gradient is shaded in 3 K/100 km increments beginning at 3 K/100 km.

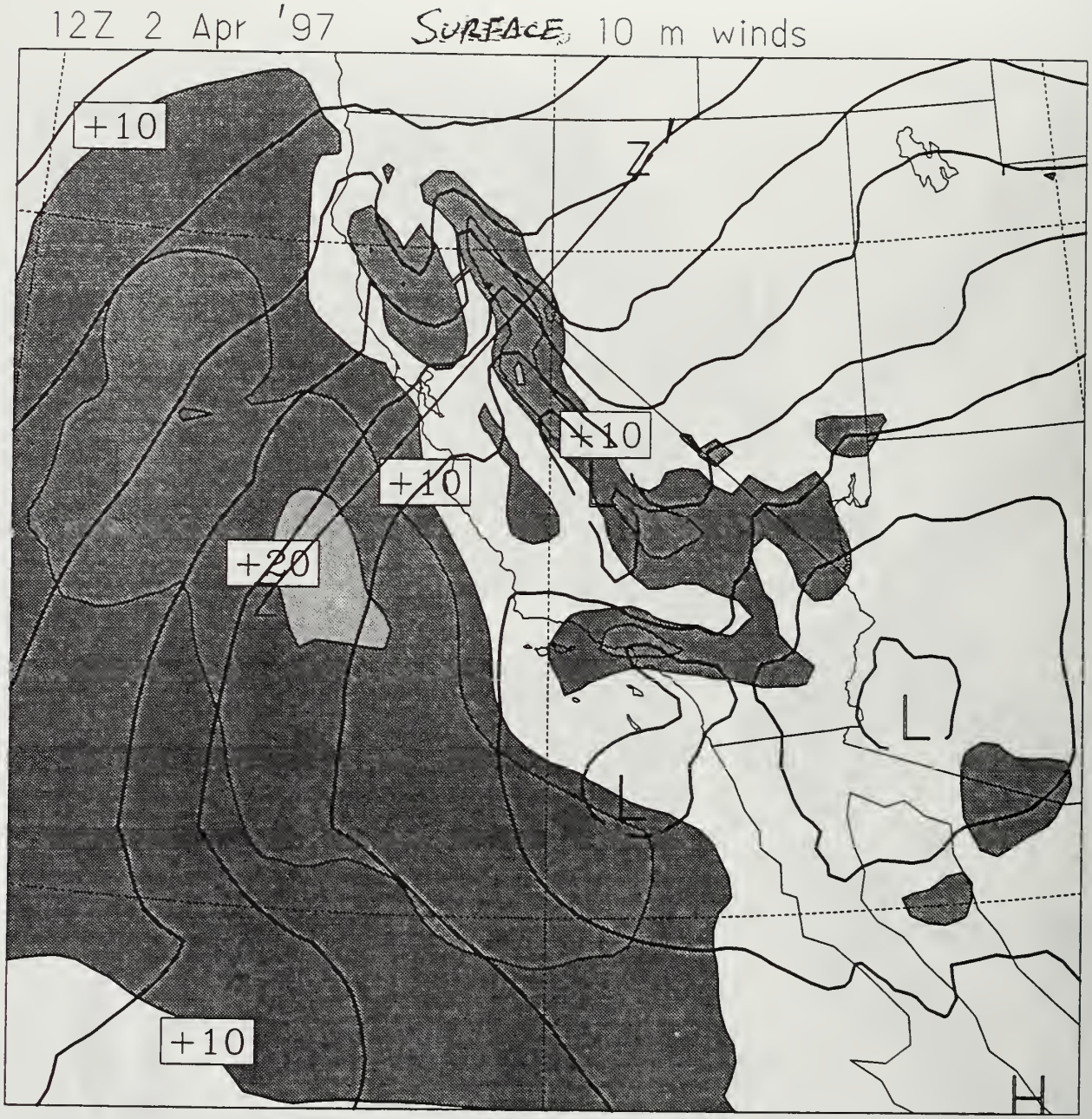

Fig. 40. COAMPS surface chart at 1200 UTC 2 April 1997. Isobars are solid lines (4 mb increment). Cross section location denoted by line Z to Z'. 10 m isotachs are shaded in 5 m/s increments starting at 10 m/s.

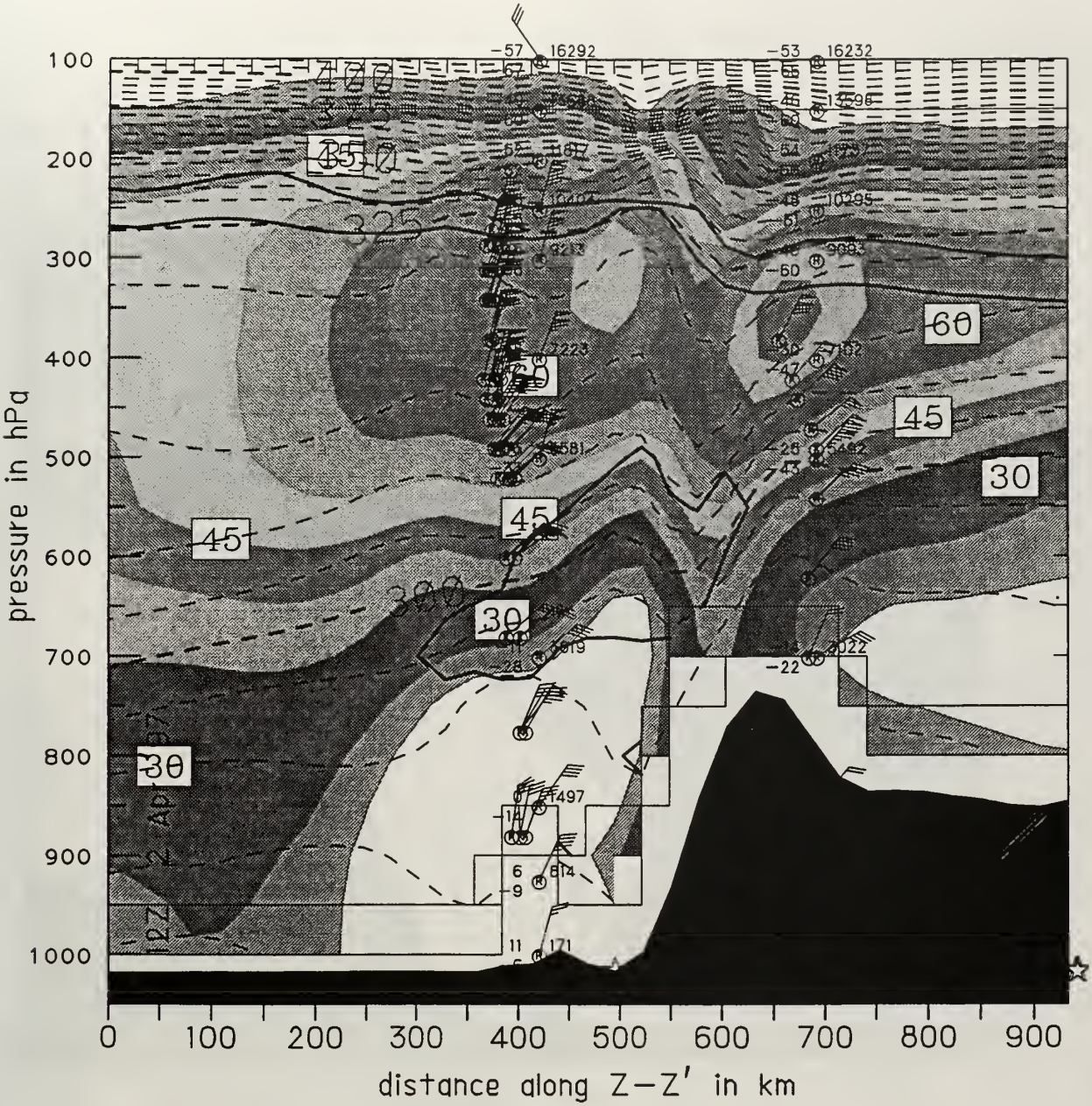

Fig. 41. COAMPS cross section at 1200 UTC 2 April 97 through the Z to Z′ plane identified in Fig. 40. Cross section details same as in Fig. 4.

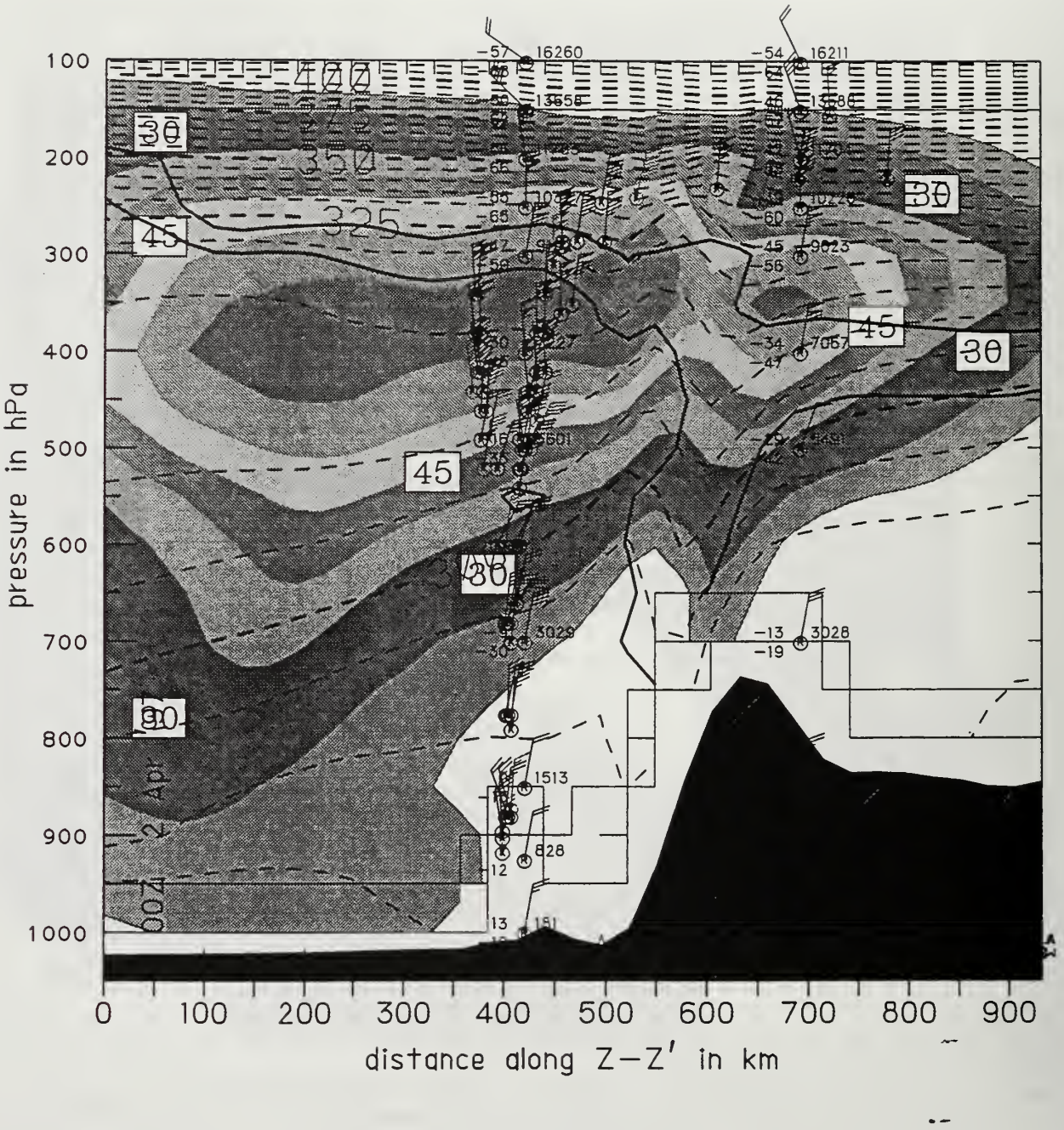

Fig. 42. Same as Fig. 41 except for 0000 UTC 2 April 1997.

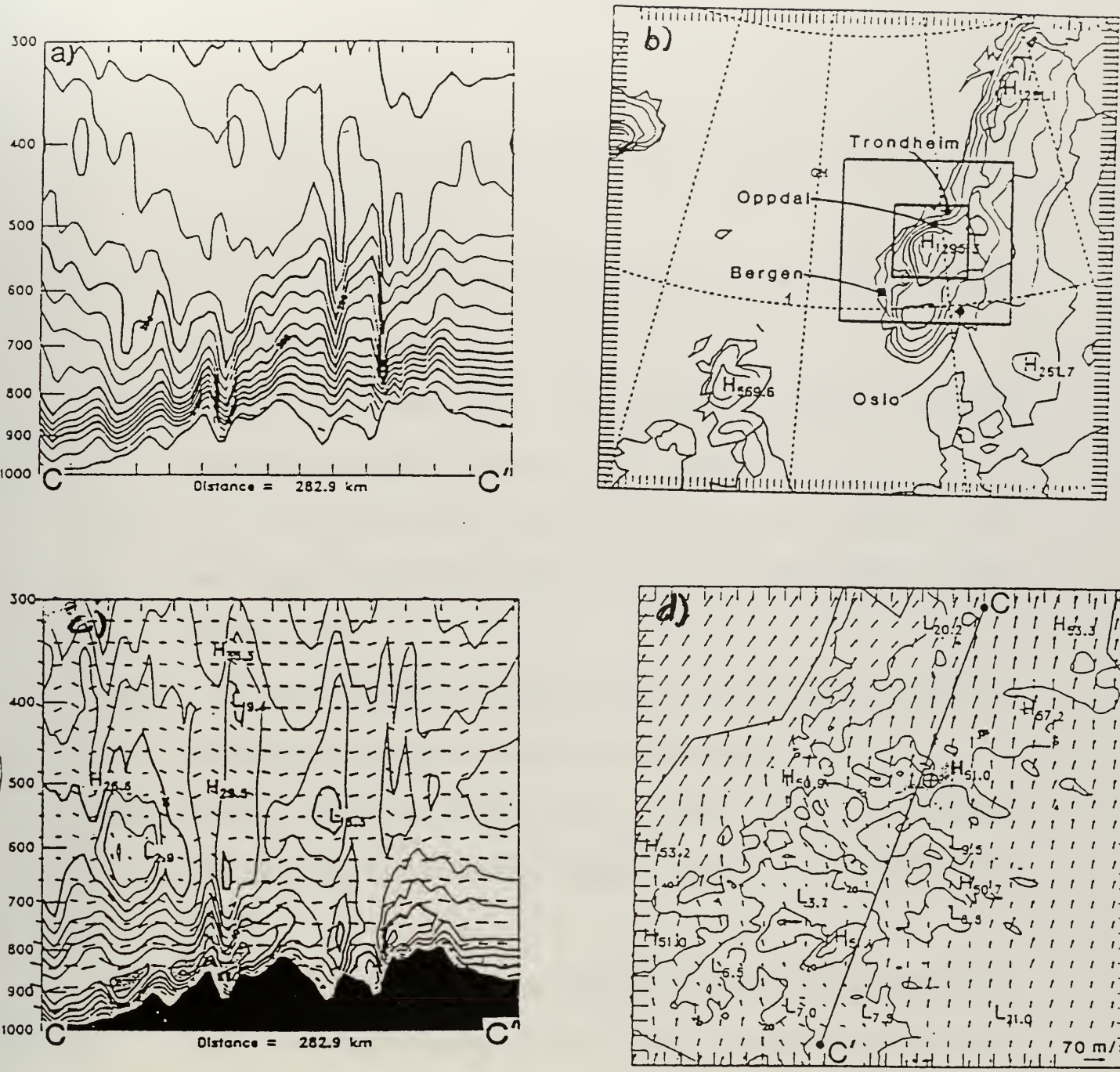

Fig. 43. Diagrams from Doyle et al. 1995. a) is isentropic cross section, b) is topographic and COAMPS grid map, c) is cross section of horizontal wind speed in m/s; d) is plan view of cross sectional plane C to C′.

LIST OF REFERENCES

Baker, N. L., 1992: Quality control for the U.S. Navy operational database. *Wea. Forecasting,* **7,** 250-261.

Barker, E. H., 1992: Design of the navy's multivariate optimum interpolation analysis system. *Wea. Forecasting,* **7,** 220-231.

Deardorff, J. W., 1980: Stratocumulus-capped mixed layers derived from a three-dimensional model. *Bound.-Layer Meteor.,* **18,** 495-527.

Doyle, J. D., M. Shapiro, and R. Hodur, 1995: A multiscale simulation of a topographically induced downslope windstorm over Norway using the navy's COAMPS model.

Durran, D. R., 1990: Mountain waves and downslope winds. *Atmospheric Processes Over Complex Terrain,* W. Blumen, Ed., Amer. Meteor. Soc., 59-81.

Harshvardhan, R. Davies, D. Randall, and T. Corsetti, 1987: A fast radiation parameterization for atmospheric circulation models. *J. Geophys. Res.,* **17,** 209-228.

Hodur, R. M., 1997: The Naval Research Laboratory's Coupled Ocean/Atmosphere Mesoscale Prediction System (COAMPS). *Mon. Wea. Rev.,* **125,** 1414-1430.

Kain, J. S., 1990: A one-dimensional entraining-detraining plume model and its application in convective parameterization. *J. Atmos. Sci.,* **47,** 2784-2802.

____, and J. M. Fritsch, 1993: Convective parameterization for mesoscale models: The Kain-Fritsch scheme. *The Representation of Cumulus Convection in Numerical Models, Meteor. Monogr.*, No. 46. Amer. Meteor. soc., 165-170.

Keyser, D., and Shapiro, M. A., 1986: A review of the structure and dynamics of upper-level frontal zones. *Mon. Wea. Rev.*, **114,** 452-499.

Lorenc, A. C., 1986: Analysis methods for numerical weather prediction. *Quart. J. Meteor. Soc.*, **112,** 1177-1194.

Louis, J. F., M. Tiedtke, and J. F. Geylen, 1982: a short history of the operational PBL-parameterization at ECMWF. *Workshop on Planetary Boundry Parameterization*, Reading, United Kingdom, ECMWF, 59-79.

Mesinger, F., 1990: "Horizontal" pressure reduction to sea level. Preprints, 21. *internationale Tagung fur alpine Meteorologie*, Engelberg, Switzerland, Schweizerische meteorologische Anstalt, 31-35.

____, and R. E. Treadon, 1995: "Horizontal" reduction of pressure to sea level: Comparison against the NMC's Shuell method. *Mon. Wea. Rev.*, **123,** 59-68.

Pauley, P. M., N. L. Baker, and E. H. Barker, 1996: An observational study of the "Interstate 5" dust storm case. *Bull. Amer. Meteor. Soc.*, **77,** 693-720.

____, 1997: An example of uncertainty in sea level pressure reduction. Submitted to *Wea. Forecasting*.

Rutledge, S. A., and P. V. Hobbs, 1983: The mesoscale and microscale structure of organization of clouds and precipitation in midlatitude cyclones. VIII: A model

for the "seeder-feeder" process in warm-frontal rainbands. *J. Atmos. Sci.*, **40,** 1185-1206.

Shapiro, M. A., and D. Keyser, 1990: Fronts, jet streams and the tropopause. *Extratropical Cyclones the Erik Palmen Memorial Volume,* C. Newton and E. O. Holopainen, Eds., Amer. Meteor. Soc., 167-191.

INITIAL DISTRIBUTION LIST

	No. Copies
1. Defense Technical Information Center 8725 John J. Kingman Rd., STE 0944 Ft. Belvoir, VA 22060-6218	2
2. Dudley Knox Library Naval Postgraduate School 411 Dyer Rd. Monterey, CA 93943-5101	2
3. Meteorology Department Code MR Naval Postgraduate School 589 Dyer Rd Rm 254 Monterey, CA 93943-5114	1
4. Oceanography Department Code OC Naval Postgraduate School 883 Dyer Rd Rm 328 Monterey, CA 93943-5122	1
5. Dr. Patricia M. Pauley Code MR/PA Naval Postgraduate School 589 Dyer Rd Rm 254 Monterey, CA 93943-5114	6
6. Dr. Teddy Holt Naval Research Laboratory 7 Grace Hopper Ave Stop 2 Monterey, CA 93943-5502	1
7. LCDR Ken Schwingshakl, USN 107 Larchwood Dr Slidell, LA 70461	1
8. Commanding Officer Fleet Numerical Meteorology and Oceanography Center 7 Grace Hopper Ave Stop 1 Monterey, CA 93943-5502	1